論文 / 著書情報
Article / Book Information

題目(和文)	
Title(English)	Study on the effect of epitaxial strain and structural stability on luminescent property of spinel oxide thin films
著者(和文)	太宰卓朗
Author(English)	Takurou Dazai
出典(和文)	学位:博士(工学), 学位授与機関:東京工業大学, 報告番号:甲第11583号, 授与年月日:2020年9月25日, 学位の種別:課程博士, 審査員:川路 均,大場 史康,平松 秀典,和田 裕之,松田 晃史
Citation(English)	Degree:Doctor (Engineering), Conferring organization: Tokyo Institute of Technology, Report number:甲第11583号, Conferred date:2020/9/25, Degree Type:Course doctor, Examiner:,,,,
学位種別(和文)	博士論文
Type(English)	Doctoral Thesis

Study on the effect of epitaxial strain and structural stability on luminescent property of spinel oxide thin films

A doctoral dissertation

Department of Materials Science and Engineering

Interdisciplinary Graduate School of Science and Engineering

Tokyo Institute of Technology

Takuro DAZAI

March 2020

Copyright

Adviser to the doctoral dissertation

Professor Hitoshi KAWAJI

CERTIFIED BY

Professor Fumiyasu OBA

Associate Professor Hidenori HIRAMATSU

Associate Professor Hiroyuki WADA

Lecturer Akifumi MATSUDA

LIST OF CONTENTS

Chapter 1.

General Introduction

1.1. Background

Light is one of the essential for our lives. For this reason, research on light has been very active, and researchers have been studying the relationship between living organisms and light, plants and light, and matter and light. In particular, the relationship between matter and light has been actively researched for a long time and applied to lighting, display devices, solar power generation, and other applications. The phenomena that occur when the light irradiates to a substance are generally reflection, refraction, and absorption. Reflections are applied to mirrors and optical fibers used in transmission equipment, while refraction is used in lenses and It is used in devices that convert frequencies. Absorption is directly affected by the matter. For example, when the light irradiated to the matter, the matter emits light with different wavelengths or gets warm. And, by observing the generation of heat or light emission from the material caused by absorbed light, I can know the nature of the material. In general, a phosphor is a material that emits luminescence in response to external stimuli such as light, heat, sound, stress, and so on (shown in Fig.1-1). Phosphors can be classified into two main categories. One is the luminescence from the crystal itself, such as interband luminescence and donor-acceptor pair luminescence. The other is to add a transition metal or a rare earth metal to the host material as a luminescent center, and then to use it to emit light from the luminescent center. Advances in semiconductor technology have mainly been based on the former, which has led to widespread research using thin films. On the other hand, phosphors doped with transition metal ions and rare-earth metal ions can be used in lighting and display devices, and therefore, research on thin films and nanoparticles has begun to be actively investigated [2-5]. Practical phosphors are required to have various characters. For example, the phosphor used in light emitting diodes (LEDs) were demanded the thermal stability because the temperature of high-power white LEDs become high temperature [6]. In addition, high color rendering is required in order to obtain like sunlight. [5]. In the field emission display (FED),

materials need chemical stability and electron conductivity since phosphor was bombarded by electrons [7]. Bioimaging phosphor needs non-toxicity and a long lifetime which is over 10 minutes, and such phosphors are called persistent (afterglow) phosphors [8]. In this way, many researchers have made various improvements according to their application. However, various phosphors have not been developed based on clear material search guidelines, but have been developed by countless trials and errors and accidents. Therefore, it was difficult to summarize the essence of phosphor materials universally and uniformly. In recent years, research on garnet-type compounds centering on YAG ($Y_3Al_5O_{12}$) has been actively conducted [9-12]. One of the key points of interest for this material is that it has a wide compositional range without changing its crystal structure. Such research has made it possible to systematically adjust characteristics such as thermal quenching temperature and afterglow time, making it easier to set guidelines for material design. Similar research has been actively conducted on perovskite-type compounds, and it has become clear that the energy position of the local emission center in the material is important [13-16]. In this way, research on phosphors has been systematically performed in the last decade, and it is thought that the discovery of factors leading to an increase in luminous efficiency will soon come. Therefore, it is necessary to search for the luminescent properties of a material with a different crystal structure. In this study, I focused on spinel compounds, which are considered to be highly applicable as luminescent materials along with perovskite and garnet compounds.

1.2. Thin film application of phosphor

When considering the application of phosphors, it is required that the size of various materials become nanoscale in order to miniaturize devices. In the field of display, cathode-ray tube (CRT) replaced flat panel displays (FPDs) such as electroluminescence (EL) or FED. In many powder phosphors, if the particle size becomes too small, the emission efficiency is lowered, so it is often used in the range of 5-10 μm. However, considering the application to FPDs, smaller particle shape is required. Therefore, researches on nanoparticle phosphors have been actively conducted [17, 18]. On the other hand, thin film phosphors have many advantages for device applications. For example, when applying to FED, the conductivity of the material is important. For this reason, the resistance value can be greatly reduced by changing the shape of a thin film. Moreover,

it can be expected that a stable luminance can be obtained by producing a uniform thin film such as an epitaxial thin film. In addition, EL materials require high-quality thin films in order to apply an electric field uniformly. Especially perovskite-type oxides, which have been studied extensively, have been reported to emit light from materials containing rare earth metals in titanates and hafnates thin films [19-21]. Furthermore, EL light emission from $YAlO_3$ thin film doped with Gd^{3+}, which was produced with the aim of becoming the next generation ultraviolet light source, has been reported [22]. In addition, (Ca, Sr)TiO_3 has succeeded in significantly reducing the driving voltage by producing an epitaxial film [23]. As in these examples, the advantages of the formation of the epitaxial film are very great, but there are also disadvantages. One of the disadvantages is a decrease in emission intensity due to a decrease in volume. The other one is the effect of a strain. However, a strain can also be seen as an advantage. G. Bai *et al.* revealed that the emission peak of $SrTiO_3$:Ni was affected by the strain by using different thickness films and piezoelectric substrate [24]. Figs.1-2 showed the emission spectra of $SrTiO_3$:Ni thin film depending on the film thickness and DC bias voltage applied to $Pb(Mg_{1/3}Nb_{2/3})_{0.7}Ti_{0.3}O_3$ (PMN-PT), respectively. As reported in this paper, the strain also provides a means to achieve control of the emission wavelength. Although it rarely occurs with using rare earth metals, when a transition metal element is used as the luminescent center, the luminescent characters are greatly influenced by a distortion in the surrounding environment of the luminescent center. Therefore, the influence of strain should be taken into account when the phosphor thin film is used in the application device such as the display.

1.3. Spinel compounds as host materials of phosphor

While many phosphors have been studied, the material focused on in this study is spinel structure. The spinel compounds are used for cathode material in lithium-ion battery [25], superconductors [26], or magnetic materials [27-29]. The name of the spinel structure is derived from a spinel mineral ($MgAl_2O_4$). The general formula represents AB_2O_4, A and B indicated the cation which are relatively small elements [30]. The crystal structure with cubic symmetry (Space group: $Fd\bar{3}m$) shown in Fig.1-3 has two different cation sites, octahedral (16d site) and tetrahedral (8a site) position. Spinel structures can be classified according to the arrangement of cations. In normal spinel structure, A and B ions occupy

the tetrahedral and octahedral sites, respectively. On the other hand, in the inverse spinel, A ion locates in the octahedral site and B ion is distributed both tetrahedral and octahedral sites. Further, there is a random (mixed) spinel in which both cations are randomly arranged into two cation sites. When the octahedral coordination is emphasized using brackets "[ ]", each normal and inverse spinel is expressed as $A[B]_2O_4$ and $B[AB]O_4$, respectively. The octahedral and tetrahedral sites are crystallographically different, though the space group is not changed by the cation arrangement (normal/inverse). Moreover, the spinel has an oxygen (*u*-) parameter [31]. Fig. 1-4 shows the tetrahedral site in the spinel structure. A ion locates in the center of the tetrahedron and is surrounded by four oxygen ions. In the spinel structure, the oxygen is at (*u*, *u*, *u*) and can move along [111] direction. Generally, the oxygen parameter lies between 0.24 and 0.275. When the parameter equal to 0.25, the spinel structure shows an ideal structure with regular tetrahedron and octahedron. Otherwise, the tetrahedron is not deformed, but only the octahedron is deformed. In this case, only the distance between the cation and the anion change in the tetrahedron. In addition, it is also known that some spinel compounds with cation vacancies instead of cations (e.g. γ-Fe_2O_3, γ-Al_2O_3, and γ-Ga_2O_3). In these compounds which are metastable phases called defective spinel, the charge of the cation was maintained by the anion defects generated with the cation vacancies. Thus, spinel compounds have a wide composition range in order to maintain the crystal structure even when defects are introduced.

Several oxides with spinel structure that exhibit luminescence are summarized in Table 1-1 [32-35]. As shown in Table 1-1, the three types of spinel compounds, gallate, stannate, and antimonite, emitted light even without doping. In addition, these materials and aluminates are excellent as host materials of phosphor because they emit very bright and various colors when rare-earth or transition metal elements are added [36-39]. Since it shows light emission with various colors depending on the kind of doping element, it can be applied to full-color displays that require three primary colors (Red, Green, Blue). Among them, $ZnGa_2O_4$ and Mg_2SnO_4 are expected to play an active role in FED because they can be used as transparent electrodes that show transparency and electrical conductivity [40, 41]. Furthermore, $LiGa_5O_8$: Cr shows an afterglow time over 1000 h so that it can be expected to be applied as a bioimaging phosphor used in the medical field

[8]. Here, I describe in detail the two types of materials as a phosphor that I focused on in this study.

1.3.1. About $ZnGa_2O_4$

$ZnGa_2O_4$ with normal spinel structure is one of the most famous phosphors because of high bright luminescence and chemical stability. Non-doped material shows a blue luminescence [33]. Furthermore, it is also known as multi-color phosphor, which shows blue, green, and red emission in non-doped, Mn^{2+}, and Cr^{3+} doped specimens, respectively [42]. Especially, chromium doped zinc gallate was well studied due to exhibited persistent luminescence for more than 10 min [43]. Attempts have been performed to increase the lifetime by controlling defects and doping various additive elements [44, 45]. Mn-doped $ZnGa_2O_4$ which shows bright green luminescence had been investigated to apply to display devices [46]. For this reason, many reports on thin films prepared by various techniques such as sputtering [47, 48], pulsed laser deposition (PLD) [49], and sol-gel [50] have been reported. Another interesting point of this material is the change in luminescent characters due to the introduction of defects. By adjusting the amount of zinc during fabrication, afterglow time [51], emission intensity [52], and emission color change [53] were observed. Fig. 1-5 showed the color variations depending on Zn concentration in $ZnGa_2O_4$:Mn film. This change was caused that excess Zn changed the valence of manganese and promoted the production of Mn^{4+} [53]. Thus, the amount of Zn in $ZnGa_2O_4$:Mn has a great influence on the luminescent characteristics. However, the light emission from $ZnGa_2O_4$:Mn without Zn ion, in other words, γ-Ga_2O_3:Mn has not been confirmed. It was considered that there are various reasons such as change of valence of manganese ion and formation of non-radiation center, but the exact reason has not been clarified yet. Furthermore, an interesting point of this material is that Mn^{2+} ion was able to locate in both octahedral and tetrahedral sites. The spectral shape was changed by annealing temperature as shown in Fig.1-6. This reason was an effect of the difference in the strength of the crystal field between octahedron and tetrahedron. Usually, Mn^{2+} was coordinated to the tetrahedral site [52-54]. However, since the distribution of each ion changes depending on the preparation conditions, such a change in the emission spectra occurred. As mention above, for this material to have many interesting points, especially defect and cation distribution, a more detailed investigation

can be conducted using thin film.

1.3.2. About A_2SnO_4(*A*=Mg, Zn)

Among materials with spinel structure, a stannate spinel is an interesting material. Zn_2SnO_4 (ZTO) has an inversed spinel structure and is expected to be applied as sensing [55, 56], photocatalytic material [57], or transparent conductor [58]. Moreover, ZTO has been reported to exhibit unique properties as a phosphor, which showed complex photoluminescence (PL) spectra. In addition to reports on blue-green emission [59], there were studies of luminescence with yellow-orange color from ZTO [34]. Furthermore, ZTO is very useful as a host material of phosphor into which rare-earth (Eu^{3+}) and transition metal (Cr^{3+}) is doping. [60, 61]. On the other hand, Mg_2SnO_4 (MTO) is attracting more attention as a phosphor than ZTO. Non-doped MTO showed bright blue emission [34]. Various transition metals can be added as the luminescent center, and bright emission from blue-green to red can be observed by doping Ti^{4+}, Mn^{2+}, and Co^{2+} [62-64]. Compared to other phosphors, these stannates are interesting materials because they have not been deeply researched. Of particular interest is manganese doped material. Usually, ZTO:Mn was not shown the luminescence. However, the green light emission was observed with an increase in the amount of Mg substitution (shown in Fig. 1-7) [65]. The expression of this luminescence was still unclear and further research is expected. There are few reports on the fabrication of thin films, most of which are related to ZTO, and very little about MTO thin films [58, 66, 67]. Therefore, since it can be expected as a material having both transparency and conductivity, it is a very significant material to investigate the performance as a phosphor thin film.

1.4. Motivation and Objective

As mentioned above, the use of thin films when applying phosphors to displays has great advantages. Recently, thin-film phosphors have been promoted centering on perovskite-type compounds, and some knowledge has been gathered. However, there are many unclear points that change the luminescent characters, such as strain from the substrate. In this study, I focused on spinel compounds, which are expected as high-intensity luminescent materials as well as perovskite, and try tuning the optical properties using thin film technology.

I first investigated the change in luminescent characteristics of the spinel phosphor associated with the film formation. By tuning the strains on the films by changing the deposition conditions and the thickness of the films, and the effect on the optical properties of the films was observed. Next, I was talking about composition dependence on luminescent properties. One of the advantages of thin films, there is the advantage that metastable compounds such as γ-phase Ga_2O_3 can be obtained by adjusting the preparation conditions. By taking this advantage, I prepare materials that are difficult to synthesize in bulk and investigate how their luminescent properties depend on their composition and show that the luminescent properties can be changed by controlling their composition. Finally, I try to control the luminescent properties by not only the composition but also the one-dimensional size effect by using a combinatorial method to synthesize thin films of varying composition at the same time.

Through the above, in this thesis, I have attempted to control the emission and the excitation wavelength of manganese-doped spinel-type phosphors by utilizing the advantages of thin film formation.

1.5. Construction of this study

This report consists of 5 chapters.

Chapter 1 provides background information on phosphors, especially spinel phosphors, and the thin film application of phosphor. In addition, the objective of this report is also described.

The effect of the strain on luminescent properties of $ZnGa_2O_4$:Mn film was reported in chapter 2. Films were prepared by pulsed laser deposition in various oxygen pressure, and its luminescent properties were investigated with changing film thickness. In this chapter, I clear the strain effect on luminescent properties of phosphor thin film with a spinel structure.

In chapter 3, tailoring the coordination of luminescent center in $ZnGa_2O_4$:Mn films by controlling cation deficiency was discussed. By using thin film stabilization, this chapter presented the results of the effect of Zn concentration on emission properties in

manganese doped gallium-based spinel oxide.

Chapter 4 presents that the green emission was observed from the composition spread Zn_2SnO_4-Mg_2SnO_4:Mn film. By tuning bandgap using the advantages of combinatorial methods and film techniques, I try to observe a luminescence from compositions that cannot observe the emission from bulk ceramics.

The opinion and suggestions about overall studies were concluded in chapter 5.

Table. 1 The luminescence of spinel compounds [32-35]

Composition	Emission color	Reference
$CdGa_2O_4$	Yellow-green	[32]
$LiGa_5O_8$	Blue	[33]
$ZnGa_2O_4$	Blue	[33]
Mg_2SnO_4	Blue-green	[34]
Zn_2SnO_4	orange	[34]
$LiZnSbO_4$	Blue	[32]
$Zn_7Sb_2O_{12}$	Orange	[32]
β-Ag_2MoO_4	Blue-green	[35]

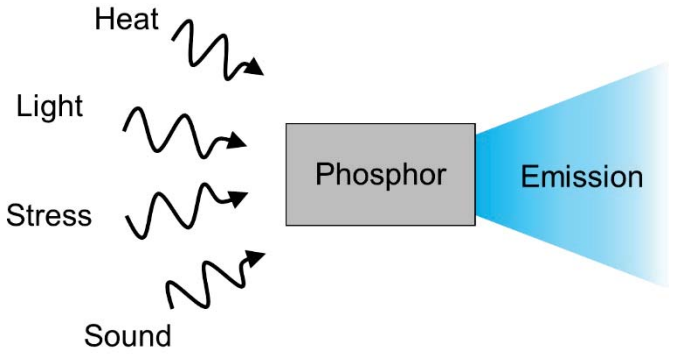

Fig.1-1 Phosphor materials

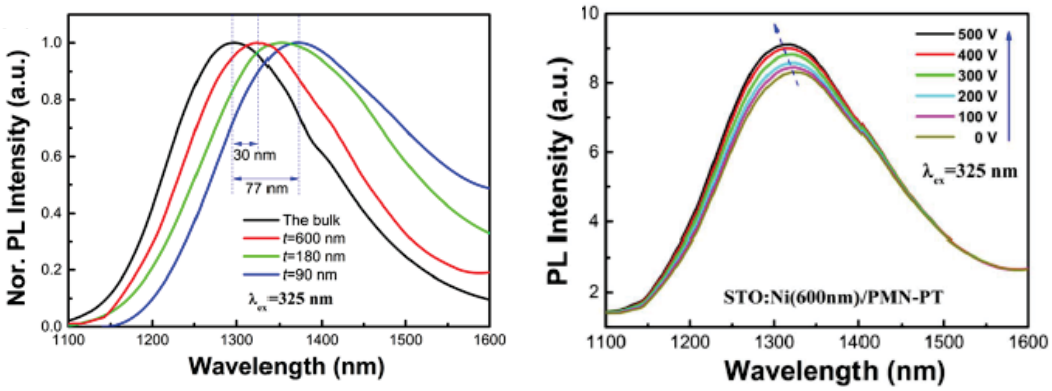

Figs. 1-2 The emission spectra of $SrTiO_3$:Ni thin film depending on (Left) the film thickness, and (Right) DC bias voltage applied to PMN-PT reported by G. Bai *et al.* [24]

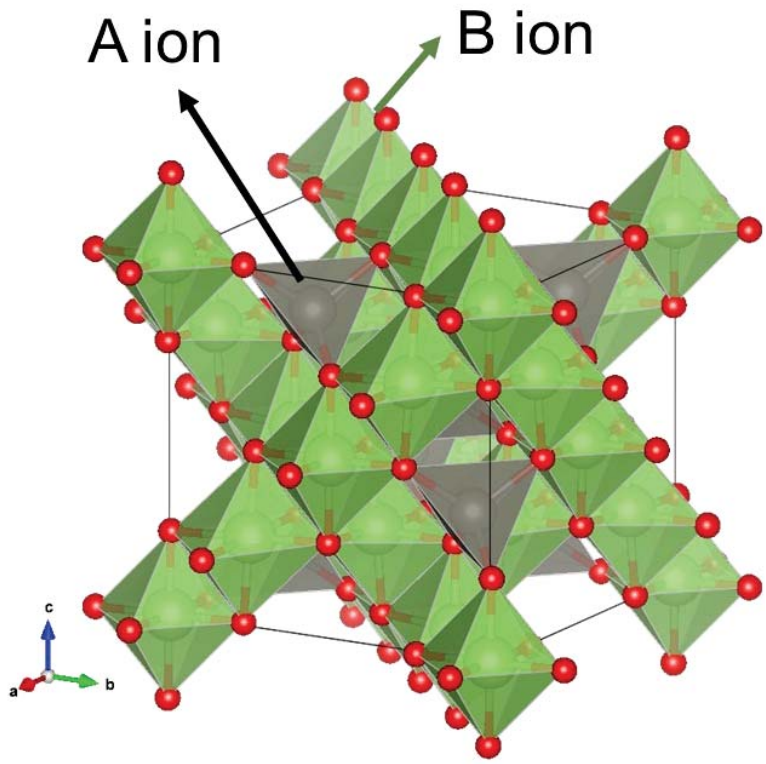

Fig. 1-3. Spinel structure (Normal arrangement) drawn by VESTA [68]

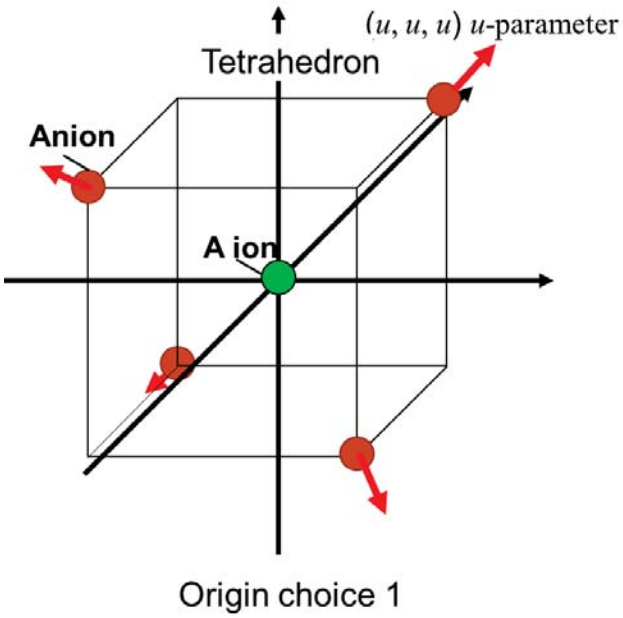

Fig. 1-4 Tetrahedron in spinel structure with oxygen (*u*-) parameter

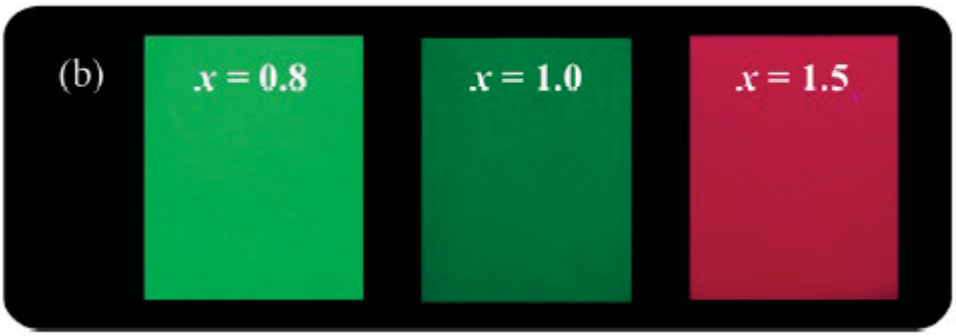

Fig. 1-4. The color variation depending on Zn concentration in $ZnGa_2O_4$:Mn film reported by Y. Wakui *et al.*[53]

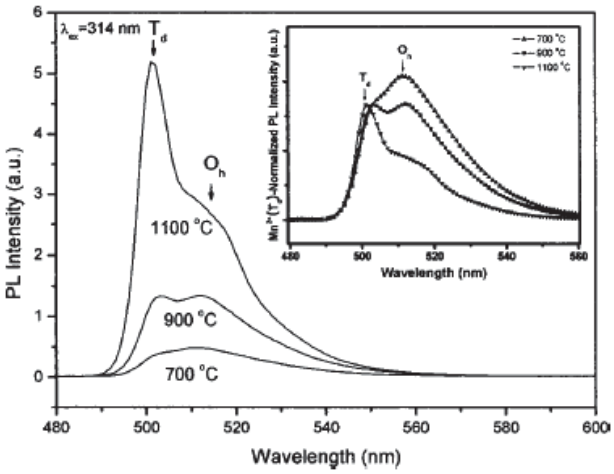

Fig. 1-5. Mn^{2+} emission from two different sites (Octahedron: Oh, tetrahedron: Td) in $ZnGa_2O_4$ reported by T. K. Tran *et al.*[54].

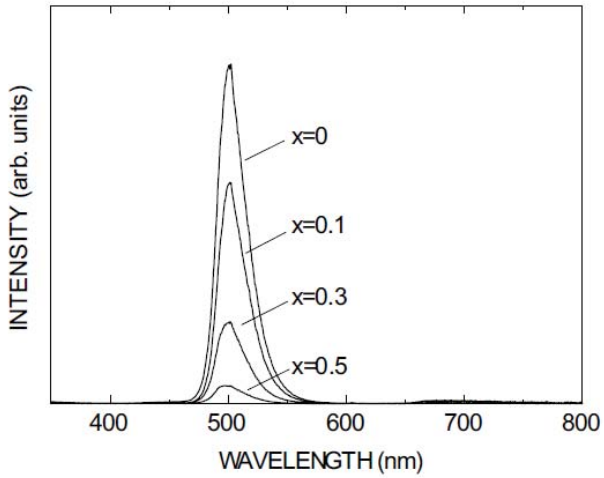

Fig. 1-6. PL spectra of $Zn_{2x}Mg_{2(1-x)}SnO_4$:Mn in synthesized by the millimeter wave heating reported by M. Kitaura *et al.*[65].

1.6. Reference

[1] S. Shionoya, and W.M. Yen (Eds.), Phosphor Handbook, CRC Press, Boca Raton, FL, (1998).

[2] YC. Lin, M. Karlsson, and M. Bettinelli, *Top Curr. Chem. (Z).* **374** (2016) 21

[3] R. S. Liu (Eds.), Up conversion Nano Particles, Quantum Dots and Their Applications, In G. Li, and J. Li, Phosphors for Field Emission Display: Recent Advances in Synthesis, Improvement, and Luminescence Properties, *Springer,* (2016) 41-82

[4] P. H. Holloway, T.A. Trottier, B. Abrams, C. Kondoleon, S. L. Jones, J. S. Sebastian, and W. J. Thomes, *J. Vac. Sci. Technol. B*, **17** (1999)758

[5] Z. Xia, Z, Xu, M. Chen, and Q, Liu, *Dalton Trans.*, **45** (2016) 11214

[6] Y. H. Kim, P. Arunkumar, B. Y. Kim, S. Unlthrattil, Eden Kim, S.H. Moon, J. Y. Hyun, K. H. Kim, D. Lee, J.S. Lee, and W. B. lm, *Nature Mater.*, **16** (2017) 543

[7] A. A. Talin, K. A. Dean, and J. E. Jaskie, *Sol. Stat. Electronics*, **45** (2001) 963

[8] F. Liu, W. Yan, Y.J. Chuang, Z. Zhen, J. Xie, and Z. Pan, *Sci. Reports*, **3** (2013) 1554

[9] J. Ueda, K. Kuroishi, and S. Tanabe, *Appl. Phys Lett.*, **104** (2014) 033519

[10] J. Ueda, K. Kuroishi, and S. Tanabe, *Appl. Phys. Exp.*, **7** (2014) 062201

[11] J. Ueda, P. Dorenbos, A. J. J. Bos, K. Kuroishi, and S. Tanabe, *J. Mater. Chem. C*, **3** (2015) 5642

[12] J. Ueda, P. Dorenbos, A. J. J. Bos, A. Meijerink, and S. Tanabe, *J. Phys. Chem. C*, **119** (2015) 25003

[13] P. T. Diallo, P. Boutinaud, R. Mahiou, and J. C. Cousseins, *Phys. Status Solidi A*, **160** (1997) 255

[14] N. Arai, T.W. Kim, H. Kubota, Y. Matsumoto, and H. Koinuma, *Appl. Sur. Sci.* **197–198** (2002) 402

[15] K. Ueda, T. Yamashita, K. Nakayashiki, K. Goto, T. Maeda, K. Furui, K. Ozaki, Y. Nakachi, S. Nakamura, M. Fujisawa, and T. Miyazaki, *Jpn. J. Appl. Phys.*, **45** (2006) 6981

[16] Y. Shimizu, S. Sakagami, K. Goto, Y. Nakachi, and K. Ueda, *Mater. Sci. Eng. B*, **161** (2009) 100

[17] G. Wakefield, E. Holland, P. J. Dobson, and J. L. Hutschison, *Adv. Mater.*, **13** (2001) 1557

[18] T.Maldiney, *Opt. Mater. Express*, **2** (2012) 261

[19] N. Arai, T.W. Kim, H. Kubota, Y. Matsumoto, and H. Koinuma, *Appl. Sur. Sci.*, **197–198** (2002) 402

[20] H. Takashima, K. Ueda, and M. Itoh, *Appl. Phys. Lett*. **89** (2006) 261915

[21] K. Ueda, T. Maeda, K. Nakayashiki, K. Goto, Y. Nakachi, H. Takashima, K. Nomura, K. Kajihara, and H. Hosono, *Appl. Phys. Express*, **1** (2008) 015003.

[22] Y. Shimizu, and K. Ueda, *Opt. Mater.*, **91** (2019) 371

[23] H. Takashima, K. Shimada, N. Miura, T. Katsumata, Y. Inaguma, K. Ueda, and M. Itoh, *Adv. Mater.*, **21** (2009) 3699

[24] G. Bai, Y. Zhang, and J. Hao, *Sci. Reports*, **4** (2014) 5724

[25] M. M. Thackeray, W. I. F. David, P. G. Bruce, and J. B. Goodenough, *Mater. Res. Bull.*, **18** (1983) 461

[26] D. C. Johnston, H. Prakash, W. H. Zachariasen, and R. Viswanathan, *Mater. Res. Bull.*, **8** (1973) 777

[27] E. J. W. Verwey, *Nature*, **144** (1939) 327

[28] L. M. Corliss, and J. M. Hastings, *J. Appl. Phys.* **33** (1962) 1138

[29] P. K. Baltzer, and J. G. White, *J. Appl. Phys.*, **29** (1958) 445

[30] O. Muller, and R. Roy, “The Major Ternary Structural Families.” *Springer-Verlag* (1974) 38-54.

[31] H. C. Neill and A. Navrotsky, *Amer. Mineral.*, **68**(1983)181

[32] G. Blasse, and A. Bril, *Mat. Res. Bull.*, **5** (1970) 231

[33] W. L. Wanmaker and J. W. ter Vrugt, and R. Roy, *J. Electrochem. Soc.*, **116** (1969) 871

[34] Y. Kotera, T. Sekine, and M. Yonemura, Bull. Chem. Soc. Jpn., **29** (1956) 616

[35] S. K. Gupta, P. S. Ghosh, K. Sudashan, R. Gupta, P. K. Pujari, and R. M. Kadam, *Dallton Trans.*, **44** (2015) 19097

[36] S. S. Pitale, V. Kumar, I. Nagpure, O.M. Ntwaeaborwa, and H.C. Swart, *Cur. Appl. Phys.*, **11** (2011) 341

[37] N. T. Melamed, P. J. Viccaro, J. O. Artman, and F. S. Barros, *J. Lumin.*, **1-2** (1970) 348

[38] T. Abritta, N. V. Vugman, and F. S. Barros, *J. Lumin.*, **31-32** (1984) 281

[39] B. S. Barros, P. S. Melo, R. H. G. A. Kiminami, A. C. F. M. Costa, and S. Alives Jr, *J. Mater. Sci.*, **41** (2006) 4744

[40] S. Itoh, H. Toki, Y. Sato, K. Morimoto, and T. Kishino, *J. Electrochme. Soc.*, **138** (1991) 1509

[41] K. N. Kim, H. Jung, H. D. Park, and D. Kim, *J. Inform. Disp.*, **2** (2001) 13

[42] Z. Gu, F. Liu, Z. Li, J. Howe, J. Xu, Y. Zhao, and Z. Pan, *J. Phys. Chem. Lett.*, **1** (2010) 354

[43] A. Bessière, S. Jacquart, K. Priolkar, A. Lecointre, B. Viana, and D. Gourier, *Opt. Express*, **19** (2011) 10131

[44] J. Su, S. Ye, X. Yi, F. Q. Lu, X. B. Yang, and Q. Y. Zhang, *Opt. Mater. Express.*, **7** (2017) 734

[45] Y. Zhuang, J. Ueda, and S. Tanabe, *Appl. Phys. Express*, **6** (2013) 052602

[46] T. Minami, T. Maeno, Y. Kuroi, and S. Takata, *Jpn. J. Appl. Phys.*, **34** (1995) L684

[47] S. M. Chung, S. H. Han, and Y. J. Kim, *Mater. Lett.*, **59** (2005) 786

[48] C. F. Yu, and P. Lin, *Jpn. J. Appl. Phys.*, **35** (1996) 5726

[49] Y. E. Lee, D. P. Norton, and J. D. Budai, *Appl. Phys. Lett.*, **74** (1999) 3155

[50] Z. Yan, M. Koike, and H. Takei, *J. Cryst. Growth*, **165** (1996) 183

[51] K. Uheda, T. Maruyama, H. Takizawa, and T. Endo, *J. Alloys. Compd.*, **262-263** (1997) 60

[52] KH. Hsu, MR. Yang, and KS. Chen, *J. Mater. Sci.: Mater.*, **9** (1998) 283

[53] Y. Wakui, Y. J. Shan, K. Tezuka, H. Imoto, and M. Ando, *Mater. Res. Bull.*, **90** (2017) 51

[54] T. K. Tran, W. Park, J. W. Tomm, B. K. Wagner, S. M. Jacobsen, C. J. Summers, P. N. Yocom, and S. K. McClelland, *J. Appl. Phys.*, **78** (1995) 5691

[55] I. Stambolova, K. Konstantinov, D. Kovacheva, P. Peshev, and T. Donchev, *J. Solid State Chem.* **128** (1997) 305.

[56] J.H. Yu, and G.M. Choi, *Sensors Actuators B Chem.* **72** (2001) 141

[57] X. Fu, X. Wang, J. Long, Z. Ding, T. Yan, G. Zhang, Z. Zhang, H. Lin, and X. Fu, *J. Solid State Chem.* **182** (2009) 517

[58] Y. Sato, J. Kiyohara, A. Hasegawa, T. Hattori, M. Ishida, N. Hamada, N. Oka, and Y. Shigesato, *Thin Solid Films.* **518** (2009) 1304

[59] J.X. Wang, S.S. Xie, Y. Gao, X.Q. Yan, D.F. Liu, H.J. Yuan, Z.P. Zhou, L. Song, L.F. Liu, W.Y. Zhou, and G. Wang, , **267** (2004) 177

[60] M. Dimitrievska, T.B. Ivetić, A.P. Litvinchuk, A. Fairbrother, B.B. Miljević, G.R. Štrbac, A. Pérez Rodríguez, and S.R. Lukić-Petrović, *J. Phys. Chem. C.*, **120** (2016) 18887

[61] Y. Zhang, R. Huang, Z. Lin, J. Song, X. Wang, Y. Guo, C. Song, and Y. Yu, *J. Alloys Compd.*, **686** (2016) 407

[62] JC. Zhang, QS. Qin, MH. Yu, HL. Zhou, and MJ Zhou, *Chin. Phys. B*, **20** (2011) 094211

[63] K. N. Kim, HK, Jung, H. D. Park, and D. Kim, *J. Lumin.*, **99** (2002) 169

[64] E.B. Silva Jr., A. López, S.S. Pedro, and L.P. Sosman, *Opt. Mater.*, **95** (2019) 109202

[65] M. Kitaura, S. Tani, S. Mitsudo, and K. Fukui, *J. Vac. Sci. Technol. B.*, **28** (2010) C2C20

[66] I. Saafi, R. Dridi, A. Mhamdi, M. H. Lakhdar, K. Boubaker, A. Amlouk, and M. Amlouk, *Optik*, **126** (2015) 4382

[67] D. L. Young, H. Moutinho, Y. Yan, and T. J. Coutts, *J Appl. Phys.*, **92** (2002) 310

[68] K. Momma and F. Izumi, *J. Appl. Crystallogr.*, **44** (2011) 1272

Chapter 2.

Strain effect on luminescent property of $ZnGa_2O_4$:Mn film

2.1. Introduction

Phosphor materials have been investigated for a long time. In recent years, the size of various materials has become nanoscale in order to miniaturize devices. In particular, the CRT has been replaced by an FPDs due to its large size. One of the FPDs, EL devices is expected to be applied to displays and lighting. LEDs with direct current-driven were a typical example, but an alternating current-driven EL (ACEL) devices are also produced [1]. In order to develop the EL devices with high performance, high-quality thin films were essentially required to reduce energy consumption. The various materials used for LEDs were investigated using epitaxial films, which has no grain boundary like a single crystal and grows along one axis. Although the phosphor applied to ACEL required a film like a single crystal as well as LEDs, it still has not been studied enough. When the epitaxial film is applied to a practical device, the influence of strain from the substrate that may change physical and structural properties must be considered. For example, the crystal structure of $SrRuO_3$ which is electrode material changed depending on the film thicknesses [2]. In the phosphor thin films, the strain introduces the spectral shift [3]. Furthermore, the bright luminescence was exhibited from the epitaxial film due to the reduction of the grain boundary [4]. Recently, manganese doped oxide phosphor for EL devices has well investigated by Minami et al. [5-7]. However, all films grew polycrystalline due to using $BaTiO_3$ ceramics sheet as the substrate. Therefore, the effect of strain from the substrate on luminescent properties have been not unclear yet.

In this chapter, I focused on $ZnGa_2O_4$:Mn phosphors, a promising candidate for FPDs, and epitaxial thin films were prepared. In order to systematically investigate the effect of strain on luminescent properties, films of different thicknesses were prepared by varying the deposition time and oxygen pressure. It was confirmed that the luminescence spectra of the epitaxial films were affected by strain. Thus, the relationship between strain and

emission spectra of spinel phosphor was clarified.

2.2. Experimental Procedure

The manganese doped $ZnGa_2O_4$ films with 60-960 nm were prepared by pulsed laser deposition (PLD). The polycrystalline ceramics target was synthesized by the conventional solid-state reaction method using ZnO, Ga_2O_3, and MnO as raw materials. The target composition was determined 0.01MnO・1.14ZnO・Ga_2O_3 because of Zn ion had a low vapor pressure [4, 8]. The raw materials weighed in the stoichiometric ratio were mixed in an agate mortar with ethanol. The mixture was pelletized into 20 mm diameter and sintered at 1575 K for 12 h. The target was struck by a fourth-harmonic wave of Nd:YAG laser (λ= 266 nm) with frequency and fluence was 2 Hz and 2.4 J/cm2, respectively. The films were deposited on (100)$MgAl_2O_4$ substrate at 773 K under O_2 pressure of 0.2 mTorr and 100 mTorr. The mismatches between $ZnGa_2O_4$ and $MgAl_2O_4$ substrate were -3.1%.

The thickness of films was measured by surface roughness measuring instrument (Kosaka Lab. Ltd., Surfcorder ET200). The crystal structure of films was characterized by high-resolution X-ray diffraction (HRXRD) using a four-axis diffractometer (Rigaku, Smart-Lab), which has monochromatized X-rays (Cu$K\alpha_1$, λ=1.5406 Å). The Zn/Ga ratio of the films was measured by X-ray wavelength-dispersive spectroscopy (WDS) (P'Analytical, PW2404). Emission and excitation spectra were obtained by spectrofluorometer (JASCO, FP-6500).

2.3. Results and Discussions

2.3.1. Compositional and structural analysis

The thicknesses of the films were controlled by changing the deposition time from 30 min to 240 min under different oxygen partial pressure. Fig. 2-1(a) shows the change in film thickness as a function of deposition time. A linear increase in film thickness with increasing deposition time can be observed in each specimen prepared under 0.2 mTorr (ZGO0.2) or 100 mTorr (ZGO100). The growth rate of ZGO100 film was 3.97 nm/min, which was faster than the growth rate with 1.77 nm/min of ZGO0.2. As shown in Fig. 2-1 (b), the Zn / Ga molar ratio of the films having different thicknesses measured by WDS was constant regardless of the film thickness. The Zn / Ga molar ratio changed depending

on the oxygen partial pressure during film formation, and the values for ZGO0.2 and ZGO100 films were 0.3 and 0.2, respectively.

Figs. 2-2 (a) and (b) show the XRD patterns of films with different thicknesses of ZGO0.2 and ZGO100, respectively. The *004* diffraction peaks of $ZnGa_2O_4$ in all films were located at the lower angle side of the substrate peak. This result indicates that the film is oriented along the [00l] direction on the substrate surface normal. Moreover, a peak appeared around 28º with increasing thickness of ZGO100 film (indicating hollow square symbol in Fig. 2-2(b)). This peak probably attributed to $ZnGa_2O_4$ *311* diffraction.

Figs. 2-3 (a)-(f) show XRD reciprocal space mappings (RSMs) of the ZGO0.2 and ZGO100 films with different film thicknesses around *408* diffractions. XRD-RSM data indicates that all of the prepared films were epitaxially grown on the $MgAl_2O_4$ substrate. The diffraction spots of the ZGO0.2 films were almost constant with the increase of film thickness. The in-plane peak position of films and substrates was almost the same, indicating that all films were clamped by the substrate regardless of increasing thickness. In the case of ZGO100 films, diffraction spots were also in the same position compared to substrate spots. I note that new diffraction spots appeared with increased thickness. The peak as observed in Figs. 2-3 (e) and (f) corresponds to the split peak in Fig. 2-2 (b) indicated by the triangle symbol. This means that the epitaxial strain of the film was released by the increase in film thickness; the film then becomes a bulky structure. To discuss residual strain in the film, the in-plane lattice constant was detected from the XRD-RSMs. The residual strain was calculated using the following equation:

$$\text{residual strain}(\%) = \frac{a_{\text{film}} - a_{bulk}}{a_{bulk}} \times 100, \qquad (2\text{-}1)$$

where a_{film} and a_{bulk} are the in-plane lattice constants of film and bulk, respectively. 8.2742 Å and 8.2468 Å for the ZGO0.2 and ZGO100 films were used for the lattice constant of a_{bulk}, respectively [11]. Figs. 2-4 (a) and (b) show calculated residual strain vs. film thickness of ZGO0.2 (Zn/Ga = 0.3) and ZGO100 (Zn/Ga = 0.2) films, respectively. The residual strain of all ZGO0.2 films was a constant of -2.3 %. On the other hand, clamped layers had a similar residual strain of -2.0%. Relaxed layers in ZGO100 films had reduced residual strain of 0 – 0.3%. This result clearly indicates that residual strain was almost released with an increase of film thickness in ZGO100 films.

2.3.2. Luminescent properties

In the previous section, I have shown that I have succeeded in fabricating thin films with different strains by structural analysis. In this section, I investigated the change of luminescent properties by film strain. First, the emission spectra of ZGO0.2 film with different thickness shows in Fig. 2-5. The emission spectrum for each ZGO0.2 film revealed a peak at approximately 525 nm, originating from the $^4T_1$-$^6A_1$ transition of Mn^{2+} ions located in the tetrahedral site [9, 10]. In other words, the position of the luminescence peak did not shift when the film thickness was changed. This result suggests that the uniformity of the luminescence peak position with respect to the thickness of the ZGO0.2 film is due to constant strain, which revealed by structural analysis. On the other hand, conformable change was also observed in ZGO100, as shown in Fig. 2-6. In all films, the green emission of Mn^{2+} ions peaking at 508-518 nm was observed, with only a very small blueshift in comparison to the ZGO100 films. The blueshift became more significant with increasing film thickness, corresponding to the appearance of a strain-free relaxation phase. The excitation spectra also show a change in the peak position as a result of the thickness change. Details are described in Supplementary 1.

2.3.3. Discussion

Fig. 2-7 shows the emission peak positions as a function of film thickness. In the case of the ZGO0.2 film, peaks were almost constant. On the other hand, in the case of the ZGO100 film, peaks were shifted to smaller wavelengths (blue shift) discontinuously.

It was expected that the changes of luminescent properties would not be affected by Zn/Ga ratio, because the ratio of the film prepared under identical conditions remains constant (see in Fig. 2-1(b)). Therefore, it is considered that the shifts of emission peaks were affected by the residual strain from the substrate. Figs. 2-8 show the emission peak positions as a function of residual strain in the films. The peaks of ZGO100 film were shifted 10 nm when the thickness increased from 100 to 212 nm. In contrast, the peaks of ZGO0.2 films were shifted only 3 nm when the thickness increased from 100 to 425 nm. This result indicates that the emission peaks of ZGO0.2 are not shifted and those of ZGO100 are shifted to a shorter wavelength linearly, meaning that film thickness has almost no effect on emission property, which is affected only by residual strain. Even in films with the same strain, the difference in emission peak position between ZGO0.2 and

ZGO100 with different deposition conditions was almost 10 nm.

Fig. 2-9 is a Tanabe-Sugano energy diagram of d^5 in tetrahedral configuration [11]. Generally, Mn^{2+} locates at the tetrahedral site in $ZnGa_2O_4$ host material. The electronic configuration of Mn^{2+} is $3d^5$, which, as is well known, has energy that splits in the octahedral and tetrahedral crystal field, as shown in the figure. The green emission from Mn^{2+} occurs by transitions from the $^4T_1$ excitation state to the $^6A_1$ ground state. The crystal field splitting parameter of the octahedral symmetry ($D_{\text{octahedral}}$) is well known by the following equation:

$$D_{\text{octahedral}} = \frac{35Ze}{4R^5}, \tag{2-2}$$

where Z is the valence of ligand surrounded the center cation, e is the charge of the electron, and R is the length between ligand and center cation. In addition, the relation of the crystal field splitting parameter between octahedral and tetrahedral ($D_{\text{tetrahedral}}$) symmetries can be written as the following equation:

$$D_{\text{tetrahedral}} = -\frac{4}{9} D_{octahedral}, \tag{2-3}$$

suggesting that the magnitude of the energy splitting at tetrahedral symmetry is inversely proportional to R^5. In this study, strong compressive strain existed in the ZGO0.2 films and a thinner film was in ZGO100 films. In this case, octahedrons distorted and tetrahedrons shrank like inset Fig. 2-9. Hence, R was decreased compared to that of the bulk ceramics. Therefore, the magnitude of the energy splitting decreased. Moreover, R increased by releasing strain in thicker ZGO100 films. Consequently, it is considered that the emission peak shifted to a shorter wavelength.

2.4. Summary

In summary, I investigated the luminescent properties of ZGO thin films with several residual strain states in the film. High-quality epitaxial ZGO thin films were prepared on $MgAl_2O_4$ single crystal substrates by PLD technique, and the residual strain of the film was controlled by changing the film preparation conditions of oxygen gas and film thickness. ZGO0.2 film of arbitrary thickness was fixed with $MgAl_2O_4$ substrate. Conversely, ZGO100 film relaxed from the substrate with increasing thickness, and then the relaxation and strain phases coexisted. The emission peak shifted to a lower

wavelength with increasing thickness. Comparison of the luminescent properties of the thin films prepared under the two conditions revealed that the PLE peak is affected not only by strain but also by film thickness, and the PL peak is influenced only by strain. This peak shift was explained by the change in length between the Mn^{2+} ion and the surrounding oxygen ion.

2.5. Reference

[1] W. A. Thornton, *Phys. Rev.*, **102** (1956) 38.

[2] S. H. Chang, Y. J. Chang, S. Y. Jang, D. W. Jeong, C. U. Jung, Y. Kim, J. Chung, T. W. Noh, *Phys. Rev. B.*, **84** (2011) 104101.

[3] G. Bai, Y. Zhang, and J. Hao, *Sci. Reports*, **4** (2014) 5724.

[4] Y. E. Lee, D. P. Norton, and J. D. Budai, *Appl. Phys. Lett.*, **74** (1999) 3155.

[5] T. Minami, T. Miyata, S. Takata, and I. Fukuda, *Jpn. J. Appl. Phys.*, **30** (1991) L117.

[6] T. Miyata, T. Nakatani, and T. Minami, *Thin Solid Films*, **373** (2000) 145.

[7] T. Minami, T. Maeno, Y. Kuroi, and S. Takata, *Jpn. J. Appl. Phys.*, **34** (1995) L684.

[8] Y. E. Lee, D. P. Norton, J. D. Budai, C. M. Rouleau, and J. Park, *J. Electroceramics.*, **4** (2000) 293.

[9] C. F. Yu, and P. Lin, *Jpn. J. Appl. Phys.*, **35** (1996) 5726.

[10] L. E. Shea, R. K. Datta, and J. J. Brown, *J. Electrochem. Soc.*, **141** (1994) 1950.

[11] D. L. Wood, and J. P. Remelika, J. Appl. Phys., 38(1967)1038.

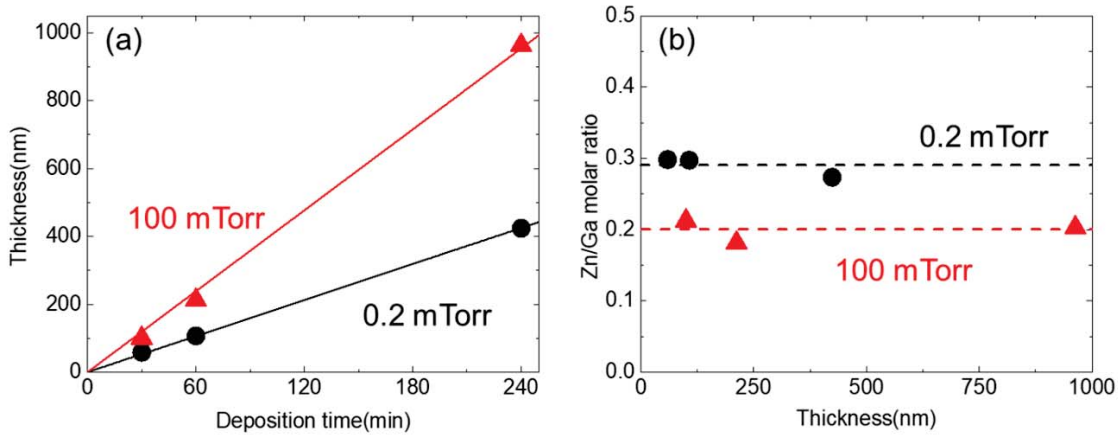

Fig. 2-1 (a) Film thicknesses of ZGO0.2 and ZGO100 as a function of deposition time, (b) Zn / Ga molar ratio of films according to thickness changes. Black circles and red triangles correspond to the films deposited under 0.2 mTorr and 100 mTorr, respectively.

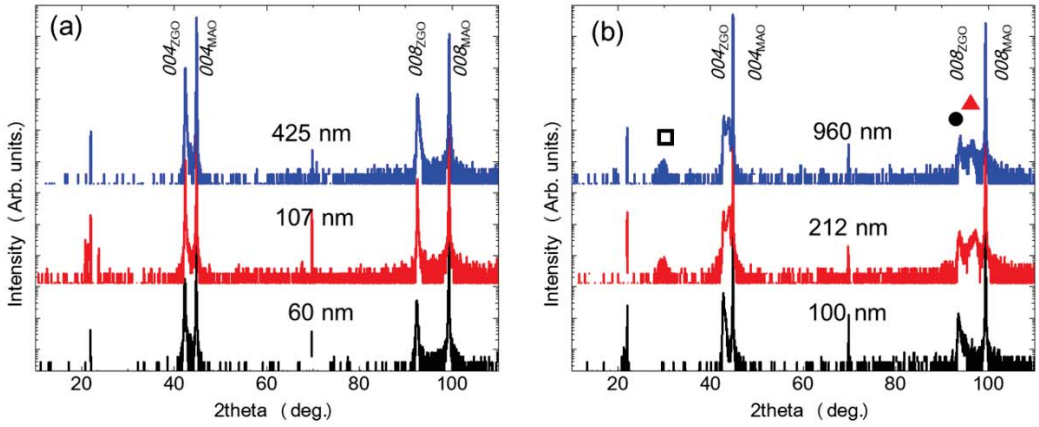

Fig. 2-2 XRD θ-2θ patterns of: (a) ZGO0.2; and (b) ZGO100 films with different thicknesses. Hollow square symbol indicates $ZnGa_2O_4$ *311* diffraction. Black circle and red triangle indicate *008* diffraction peak of strained and relaxed film, respectively.

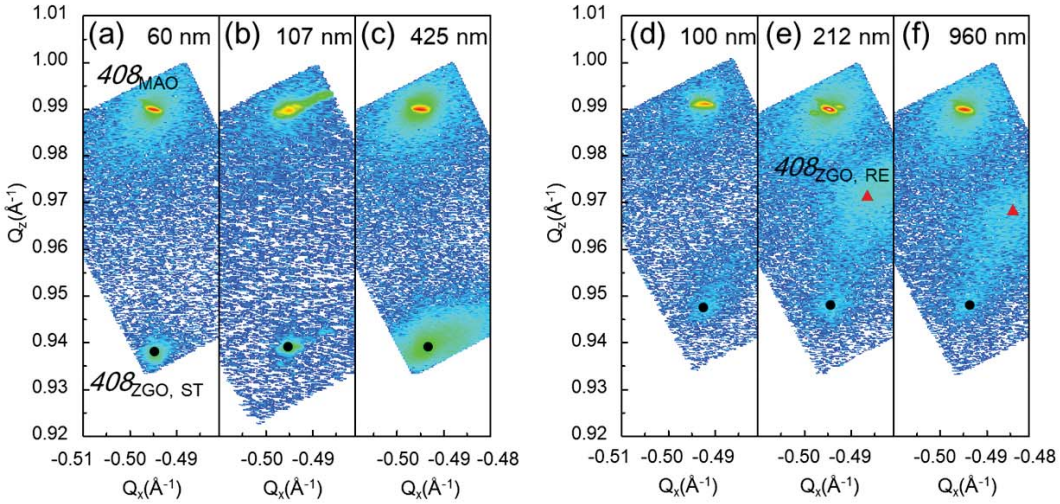

Fig. 2-3 XRD-RSMs around 408 diffraction of (a)-(c) ZGO0.2 and (d)-(f) ZGO100 films. The subscripts ST and RE indicate strained peak (black circle) and relaxed peak (red triangle), respectively.

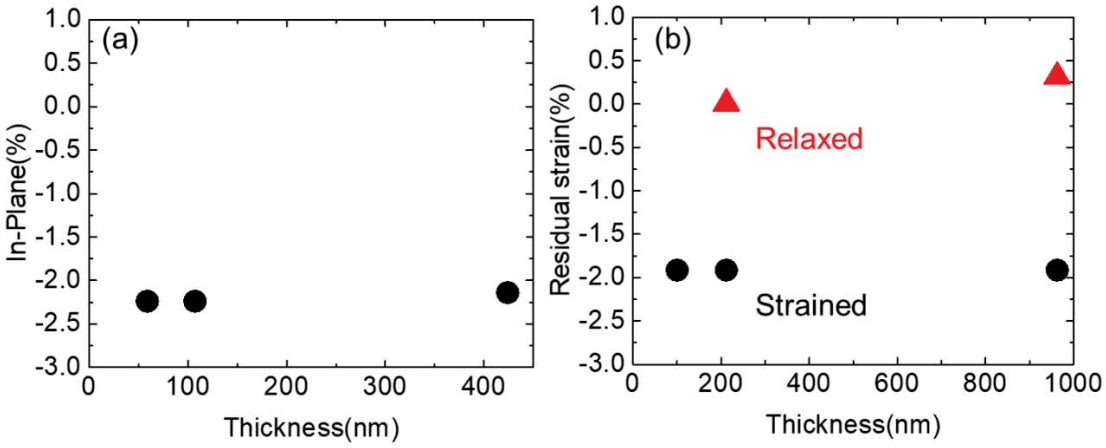

Fig. 2-4 Residual strain of (a) ZGO0.2, and (b) ZGO100 films as a function of film thickness.

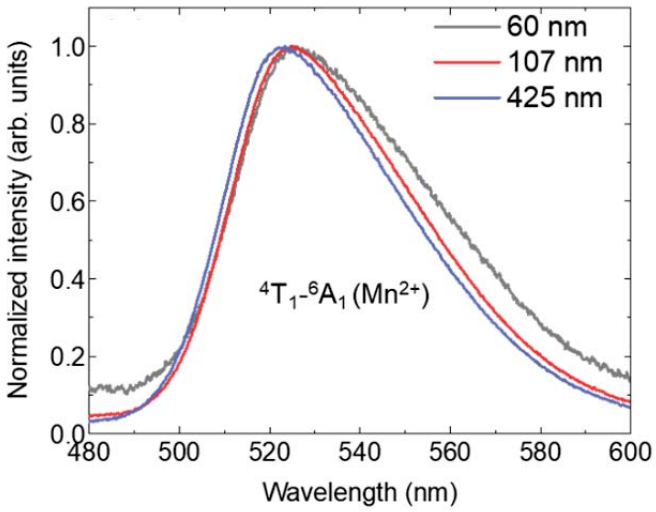

Fig. 2-5 Emission spectra of ZGO0.2 film with different thickness.

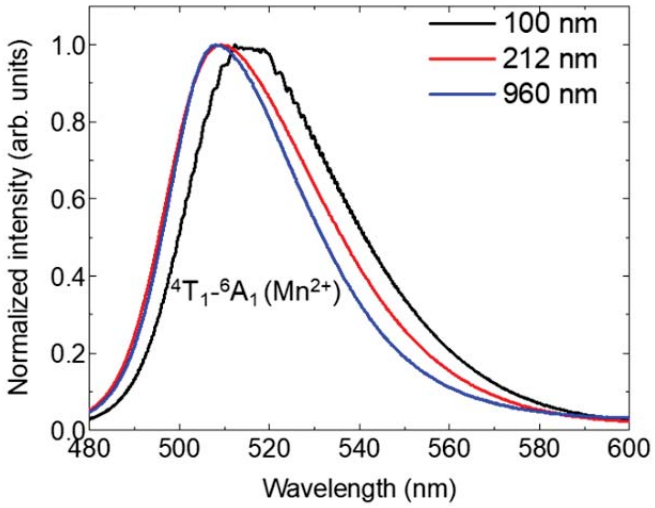

Fig. 2-6 Emission spectra of ZGO100 film with different thickness.

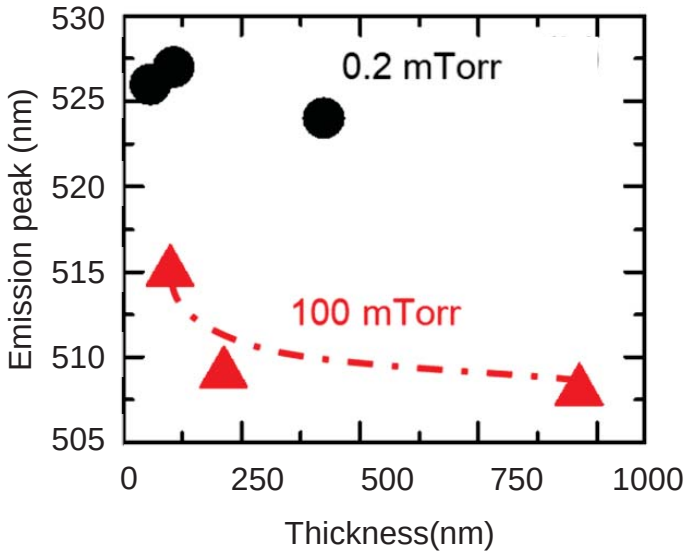

Fig. 2-7 Emission peaks as a function of film thickness. The lines in the figure were drawn by eye guide.

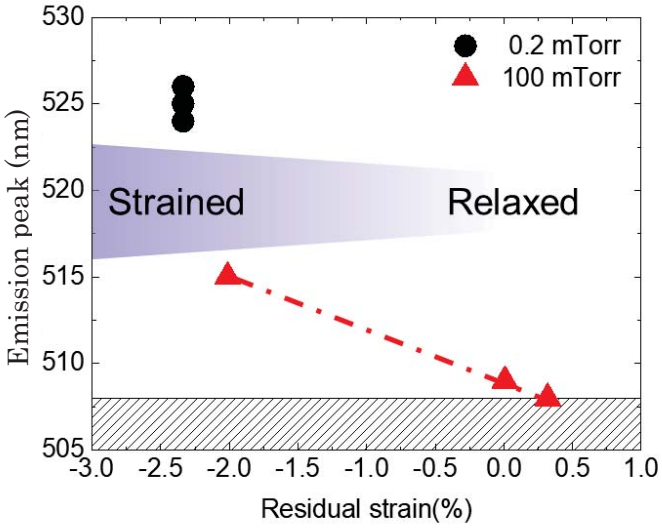

Fig. 2-8 Emission peaks as a function of residual strain in the films. The lines are drawn by eye guide. The shaded area from 505 to 508 nm corresponds to the emission peaks of polycrystalline bulk $ZnGa_2O_4$:Mn [7, 9, 10].

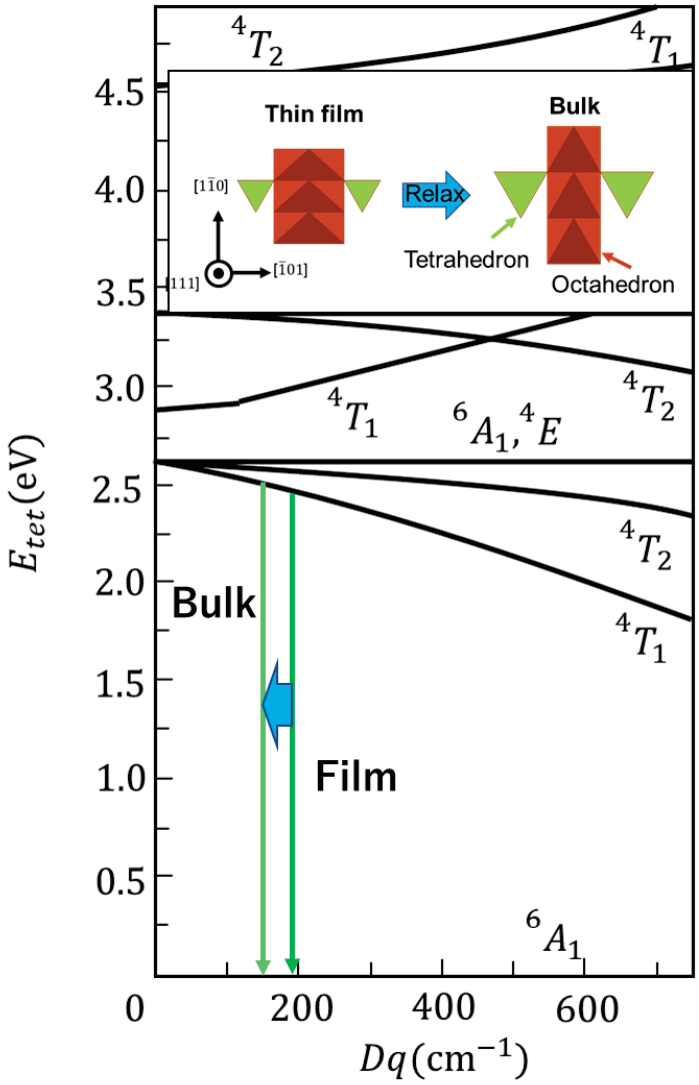

Fig. 2-9 Tanabe-Sugano energy diagram of d^5 in tetrahedral configuration [11]. Inset is a schematic image of octahedron and tetrahedron distortion during film relaxation.

Chapter 3.

The effect of Zn-deficiency in $ZnGa_2O_4$:Mn film

3.1. Introduction

In this chapter, I investigated the effect of Zn concentration in $ZnGa_2O_4$, which was briefly mentioned in chapter 2. Zinc gallate ($ZnGa_2O_4$) has a wide bandgap, a high transmittance against the ultraviolet (UV) region, and stability under the vacuum. Therefore, this material is attracted much attention for the application to electrical and optical devices, such as a deep-UV photodetector [1], EL [2], and FED [3]. In the field of electro-optical materials, the gallium-based oxide materials were also attracted as a promising candidate [4]. It is also gathering attention as a luminescent material, and many studies have been reported. Transition or rare earth metal doped amorphous Ga_2O_3 film was a candidate for an emitting layer of display devices [5, 6]. The crystalline Ga_2O_3 was also used in other display devices such as EL and FED [7, 8]. These two materials could be formed the same crystal structure which called spinel structure. Like a γ-Ga_2O_3, some spinel compounds were composed by introducing cation defects instead of cations, and they called defective spinel (e.g. γ-Al_2O_3, γ-Fe_2O_3, and γ-Ga_2O_3) [9]. The γ-phase is a metastable phase that has higher formation free energies than other phases [10]. Nevertheless, there are some reports about γ-Ga_2O_3 prepared by solvolysis [11], pulsed laser deposition (PLD) [12], and mist chemical vapor deposition [13] in recent year. In addition, γ-Ga_2O_3 can be formed a homogeneous solid solution with $ZnGa_2O_4$ [14]. In spinel compounds, it is known that the distribution of cations had a great influence on the physical properties [15]. Therefore, the influence of the change in cation distribution accompanying the introduction of defects on the luminescent characters was investigated using film prepared by PLD technique.

3.2. Experimental Procedure

$ZnGa_2O_4$: Mn thin films were fabricated on (100) $MgAl_2O_4$ substrates by PLD with a fourth-harmonic wave of a Nd:YAG laser (λ= 266 nm). The polycrystalline ceramics

target was prepared by the solid-state reaction using ZnO (RARE METALLIC Co. LTD, 99.999 %), Ga_2O_3 (RARE METALLIC Co. LTD, 99.9 %), and MnO (RARE METALLIC Co. LTD, 99.9 %) as raw materials. All materials were thoroughly mixed and sintered at 1673 K for 6 h. Composition of targets, *x*, was changed in the formula xZnO・Ga_2O_3 for x = 0, 0.25, 0.50, 0.75, and 1.0. The concentration of Mn was fixed at Mn/Ga = 0.005. The films were deposited at 773K under an oxygen pressure of 0.2 mTorr. The repetition and fluence of the laser were 2 Hz and 2.4 J/cm^2, respectively. The film thicknesses were measured by surface roughness measuring instrument (Surfcorder ET200, Kosaka Lab. Ltd.) and adjusted 65 - 80 nm. The crystal structure of the films was characterized by high-resolution X-ray diffraction (HRXRD) using a Rigaku Smart-Lab diffractometer where X-ray was monochromatized using Ge(220) 2-bounce crystal and Cu$K\alpha_1$ radiation (λ=1.5406 Å). Zn/Ga molar ratio was measured by x-ray wavelength-dispersive spectroscopy (WDS) (P'Analytical, PW2404). Optical transmittance of films deposited on both side polished substrate was measured using UV-vis spectrometer (JASCO, V-550). Photoluminescence (PL) and photoluminescence excitation (PLE) spectra were measured by spectrofluorometer (JASCO, FP-6500). The temperature dependence of PL spectra was collected by spectrofluorometer combined with the temperature-controlled stage (LINKAM, THMS600). The temperature range of measurement was from 90 to 500 K.

3.3. Results and Discussions

3.3.1. Structural and compositional analysis

The crystal structure of films prepared using targets with various Zn concentration was investigated. XRD patterns around *004* diffraction peak of films and substrate were shown in Fig.3-1 (a). The *004* diffraction peak of films was observed at around 42.5° in the low angle side of the substrate peak. In addition, no other diffraction peaks were observed in the measuring range (2θ = 10-120°). Therefore, these films were grown epitaxially with a spinel structure. Furthermore, the diffraction peak shifted toward the lower angle side with an increase in *x*. Fig. 3-1(b) showed *d*-spacing of 004 diffraction and a Zn/Ga molar ratio of the films. The *d*-spacing and the Zn/Ga ratio increased with an increase of target Zn concentration *x*. The Zn/Ga ratio of films indicated a lower value than that of targets because of the relatively high vapor pressure of Zn [16]. The *d*-spacing of the films was

larger than that of nono-particles [14]. This expansion could be explained by restraint from the substrate. The *d*-spacing estimated by considering the restrain corresponded to reference. Hereafter, the samples were referred to as "*y*ZGO". The *y* indicates Zn concentration (as twice as Zn/Ga ratio) of the films.

3.3.2. Optical properties

This change of Zn also concentration affected to an optical bandgap. Figs. 3-2(a) and (b) showed transmittance and Tauc plots of the films. The spectrum of the substrate is also shown in Fig. 3-2(a), but no significant change in the transmittance in the visible region was observed even when thin films were deposited. This result indicated that the transmittance of the thin film is very high. In the ultraviolet region, a decrease in transmittance was observed on the longer wavelength side compared to the substrate. That is, the thin film absorbs light in the ultraviolet region. In this study, assuming that the direct transitions follow the relationship of $(\alpha h\nu)^2 \propto h\nu$, Tauc plots according to the transition type were plotted using transmission spectra. The optical band gap of γ-Ga_2O_3 and $ZnGa_2O_4$ has almost the same which value is estimated at about 5.0 eV as a direct transition [13, 17]. In Fig. 3-3, the optical band gap of films indicated similar values and increased with an increase of Zn concentration. This result indicated that the optical band gap was affected by Zn concentration. From these results, the epitaxial films with spinel structure, which have various Zn concentration, was obtained in this study.

3.3.3. Luminescent properties

Figs. 3-4 (a) and (b) shows PLE and PL spectra of the films at 300 K, respectively. Fig. 3-4 (a) inset was sample images under UV irradiation (λ=254 nm). The green emission from all films without 0.00ZGO respected as γ-Ga_2O_3 was observed. The PLE spectra have a peak attributed to a host absorption of $ZnGa_2O_4$ at around 230 nm. Moreover, another peak was appeared at around 300 nm with increasing Zn concentration *y*. This peak was originated from a charge transfer absorption of Mn-O or $d^5 \rightarrow d^4s$ transition band [18]. The intensity of this peak emitted from the films was very low compared to the bulk ceramics because the volume of the film is so small that the film contained only a few amounts of Mn^{2+}. The PL spectra showed the green emission whose peak located at around 530 nm. This emission peak was assigned to $^4T_1$-$^6A_1$ transition of Mn^{2+} located in

the tetrahedral site [19]. The intensity of the peak decreased because of a reduction in the crystallinity of the film with a decrease in Zn concentration. In addition, the change in spectra shape was observed. The PL spectrum of 0.32ZGO was seemed consisting of an asymmetric single peak, while two peaks were clearly observed in the PL spectra of 0.02ZGO. Non-doped $ZnGa_2O_4$ shows a blue emission with a peak located under 500 nm [2]. If Mn^{2+} changes to Mn^{4+} which have the same electron configuration of $Cr^{3+}(3d^3)$, a red emission is observed around 700 nm. Therefore, these two peaks were attributed to the difference of the site position located Mn^{2+} ion. Generally, the green emission around 510 nm was originated from Mn^{2+} located in the tetrahedral site (Td) in the spinel structure. However, a peak has appeared at a slightly longer wavelength side when the Mn^{2+} occupied the octahedral site (Oh) by a difference of preparation conditions [15, 20]. The asymmetric PL spectrum of 0.32ZGO can be deconvoluted into at least two Gaussian components peaked at 525 and 546nm (see in Fig. 3-4(b) inset), which peaks are attributed to Td and Oh peak, respectively. Usually, the location of Mn^{2+} has been investigated by electron spin resonance (ESR) measurement. However, the ESR signal could not be obtained in this study because the volume of the film had a very small than that of bulk. The peak position of Td was located at a longer wavelength side than that of bulk ceramics. This cause is considered to be a strain effect [21]. Moreover, these two peaks were drastically changed to temperature.

3.3.4. Temperature dependence of emission property

Figs. 3-5(a)-(d) shows the temperature dependence of PL spectra. With an increase in the temperature, the luminescent intensity of all films decreased with a change in the shape of the luminescence. For each sample, Oh peak was dominant at low temperature, whereas only the Td peak was clearly observed at high temperature. The temperature dependence of luminescent intensities at Oh and Td peaks were shown in Figs. 3-5(e)-(h). The modified Arrhenius equation was employed to investigate the thermal stability,

$$I(T) = \frac{I_0}{1+c\ \exp\left(-\frac{\Delta E}{k_b T}\right)} \tag{3-1}$$

where I(T) and I_0 represents the luminescent intensity at the temperature of T and 0 K, respectively. ΔE is the activation energy of thermal quenching, and c is the constant determined by host materials. k_b is a Boltzmann's constant (= 8.629×10^{-5} eV). The fitting

curve at each peak was drawn in Fig. 3-5 (a-d). The ΔE and T_{50}, which is a temperature at $I_0/2$, of all films were estimated by equation (1) and fitting curve, respectively, and were listed in Table 3-1. The thermal quenching temperatures of each peak showed a different temperature and were independent of Zn concentration. Although it was known that there are two luminescent sites in $ZnGa_2O_4$:Mn, this is the first time that it has been shown that each site had different quenching temperatures. This result indicated that each peak was derived from the same emission center.

3.3.5. Discussion

The ratio of the intensity between Td and Oh was different in each film. Fig.3-6 showed the ratio of the luminescent intensity at the Td peak (I_{Td}) to that at Oh peak (I_{Oh}) (=I_{Td}/I_{Oh}) at 80 K. The I_{Td}/I_{Oh} ratio increased with an increase in Zn concentration *y*. Therefore, this result indicated that the Zn concentration influenced the location of Mn^{2+}.

Site occupancies of γ-Ga_2O_3 and $ZnGa_2O_4$ with spinel structure were expressed as

$$\left[\mathrm{Ga}_{\frac{3}{4}} \quad _{\frac{1}{4}}\right]^{\mathrm{IV}} \left[\mathrm{Ga}_{\frac{5}{4}} \quad _{\frac{3}{4}}\right]^{\mathrm{VI}} \mathrm{O_3Vo} \tag{3-2}$$

$$[\mathrm{Zn}]^{\mathrm{IV}}[\mathrm{Ga_2}]^{\mathrm{VI}}\mathrm{O_4} \tag{3-3}$$

, respectively, where the superscript (IV, VI) represents the coordination number of the cation site, and Vo indicated an oxygen defect. The cation vacancies preferentially located in the octahedral site compared to the tetrahedral site, though these vacancies have been randomly located in the defected-spinel structure [10]. When a point defect exists in the crystal, the defected site has a larger space than if it were fully occupied. Here, the Shannon's ionic radius of each ion is expressed as Ga^{3+} = 0.47 Å, Zn^{2+} = 0.60 Å, and Mn^{2+} = 0.66 Å at the tetra-coordinate tetrahedral site [22]. On the other hand, the ionic radius is Ga^{3+} = 0.47 Å, Zn^{2+} = 0.60 Å, and Mn^{2+} = 0.66 Å at the six-coordinate octahedral site [31], and the relationship is $Ga^{3+} < Zn^{2+} < Mn^{2+}$ at any site. In γ-Ga_2O_3 with a large number of deficiencies, since Ga ions occupy the tetrahedral site the site becomes small, and Mn^{2+} is difficult to enter the tetrahedral site. In contrast, the octahedral site has a larger space because of the large number of deficiencies. Therefore, Mn^{2+} is preferentially located in the octahedral site in γ-Ga_2O_3. Subsequently, with an increase in the Zn concentration, the space of the tetrahedral site becomes gradually large because the Zn^{2+} preferentially coordinates to the tetrahedral site. At this time, Ga ions that originally located at the

tetrahedral site move to the octahedral site, and the space of the octahedral site gradually become small. Therefore, Mn^{2+} is preferentially coordinated to the tetrahedral site. In conclusion, when the Zn concentration increase in the spinel structure, the stable site of Mn^{2+} changes from the octahedral site to the tetrahedral site. Therefore, I suggested that it is possible that cation-deficiency induced crystal-site engineering.

3.4. Summary

$ZnGa_2O_4$:Mn thin film with various Zn deficient was prepared by PLD method. All films were grown epitaxially on (100)$MgAl_2O_4$. Increasing in target Zn concentration, *d*-spacing, Zn/Ga ratio, and optical bandgap of the films increased. The films without 0.00ZGO showed the green emission originated from Mn^{2+}. The PL spectra had two peaks, which is due to the difference in the site of the luminescent center. The temperature dependence of PL spectra was measured. The change of spectral shape clearly observed with an increase in the temperature. This change is attributed to the fact that the two peaks have different thermal quenching temperatures. In addition, the spectral shape depended on Zn concentration. With an increase in Zn concentration, the luminescent intensity of the Td peak increased. This result was similar to the change in crystal-site engineering. Therefore, I suggested that it is possible that cation-deficiency induced crystal-site engineering.

Table. 3-1 Activation energy and thermal quenching temperature

	Oh		Td	
	E (eV)	T_{50} (K)	E (eV)	T_{50} (K)
0.02ZGO	0.14	248	0.13	331
0.11ZGO	0.16	252	0.22	319
0.18ZGO	0.16	266	0.24	324
0.32ZGO	0.13	248	0.19	303

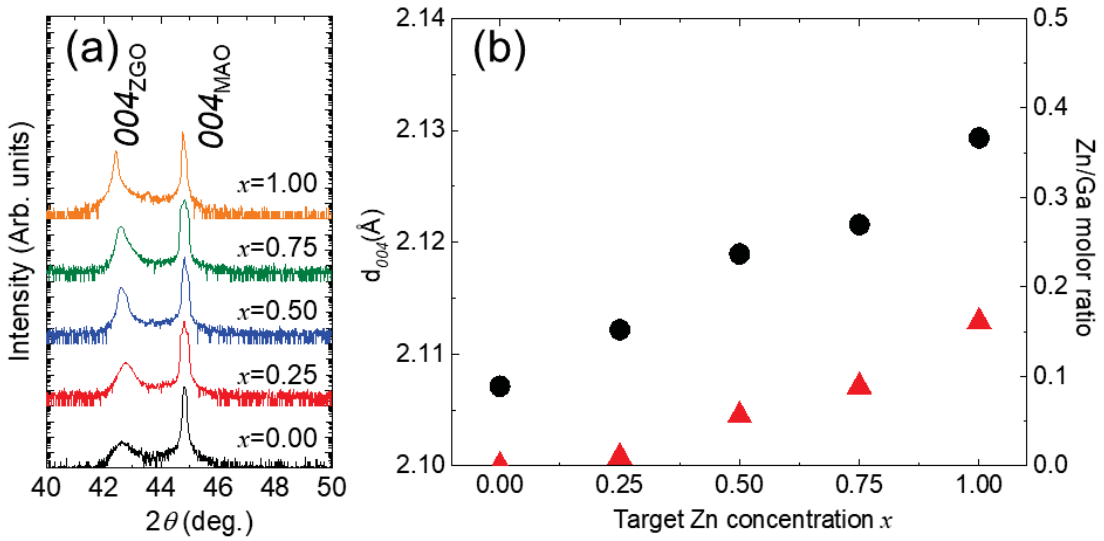

Figure 3-1. (a) XRD patterns around *004* diffraction peak of films prepared using polycrystalline targets with various Zn concentration *x*,
(b) The Zn/Ga molar ratio and d_{004} of prepared films

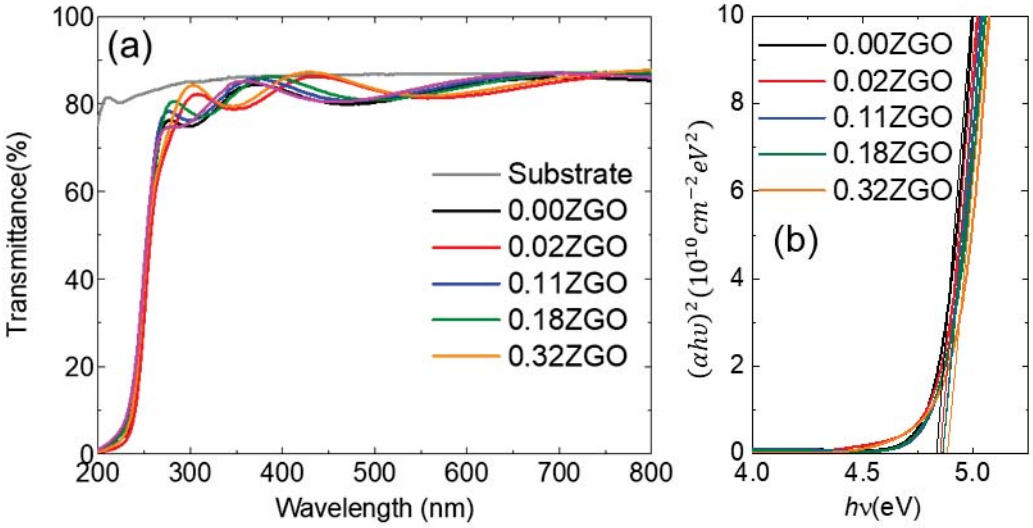

Figure 3-2 (a) Transmittance spectra of prepared films,
(b) Direct transition Tauc plots of thin films with different Zn concentrations

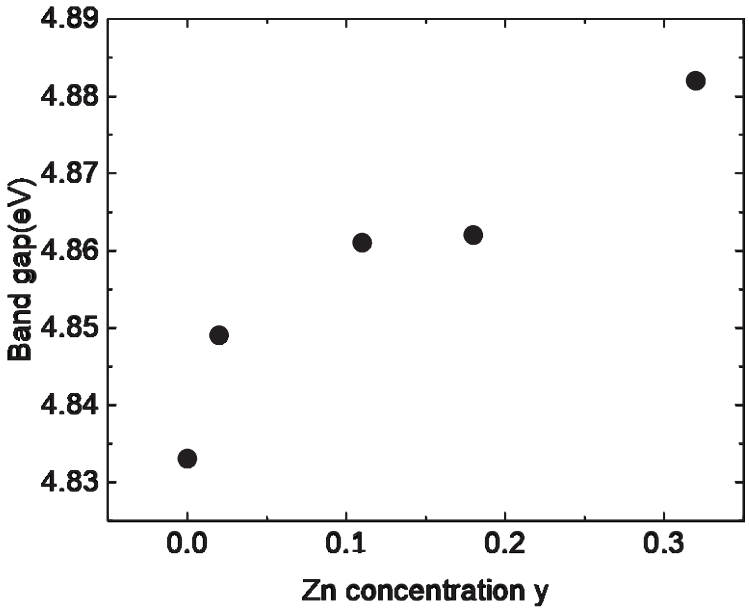

Fig. 3-3 Band gap of films estimated from Tauc plots

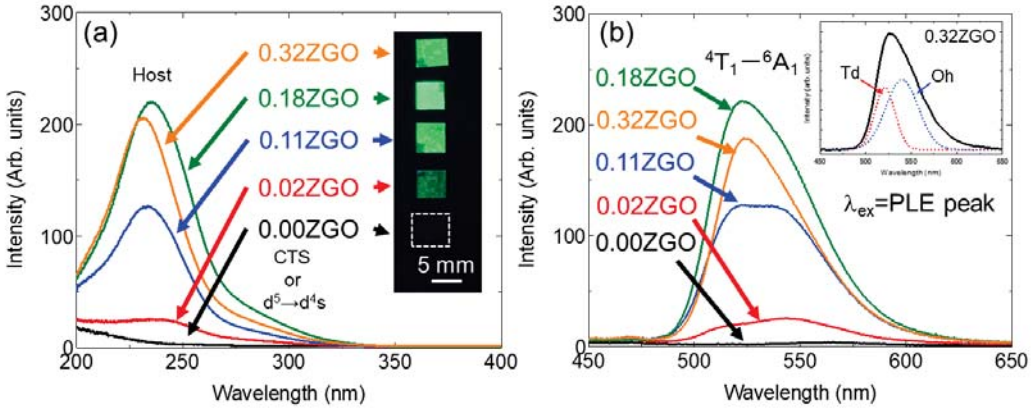

Figure 3-4(a) PLE and (b) PL spectra of *y*ZGO at room temperature,
inset Fig. 3-4(a): Images of films under the UV light,
inset Fig. 3-4(b): the Gaussian peak fitting in 0.32ZGO film

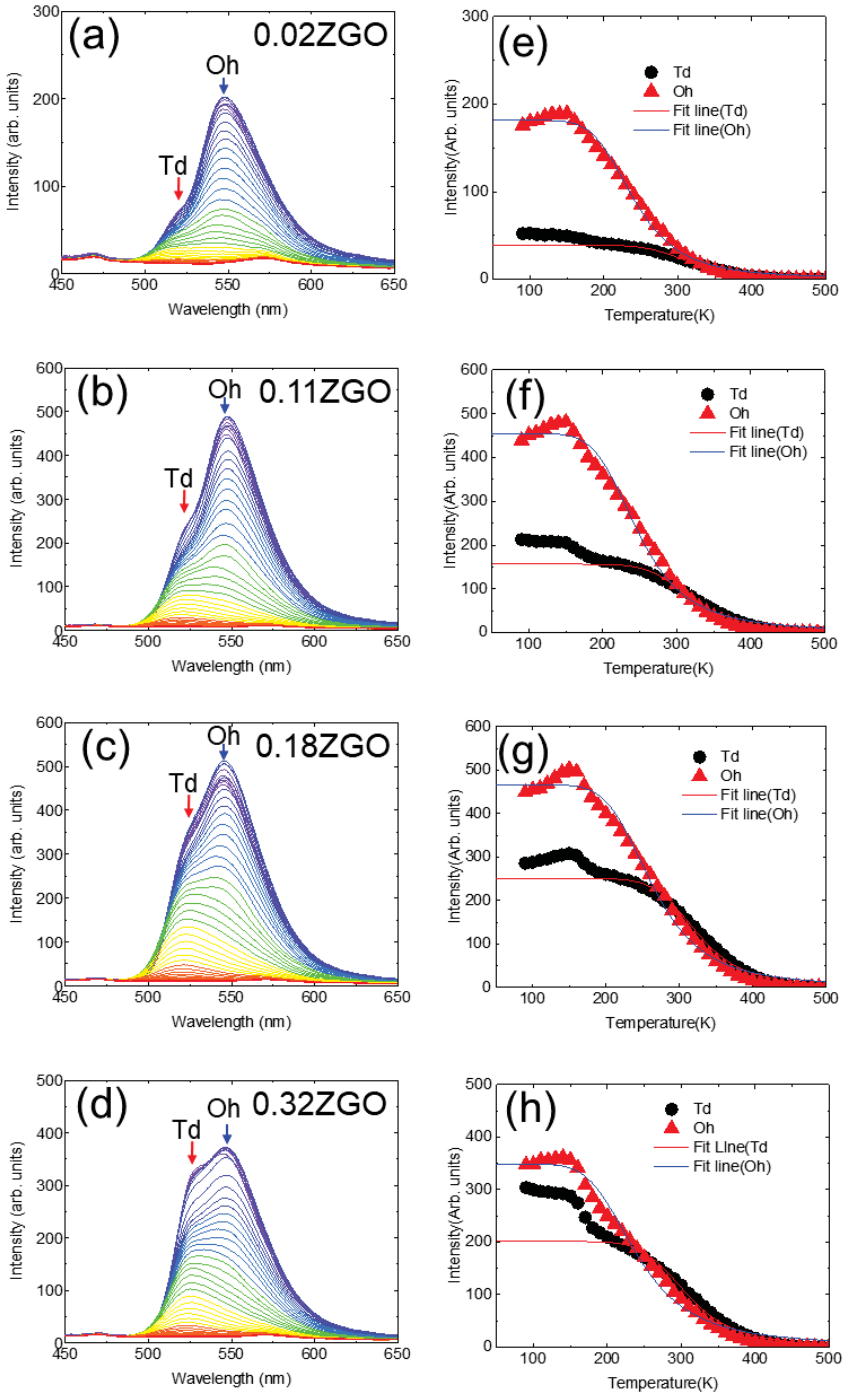

Figure 3-5. (a-d) Temperature dependence of PL spectra of *y*ZGO, (e-h) Temperature dependence of PL intensity at Td and Oh peaks

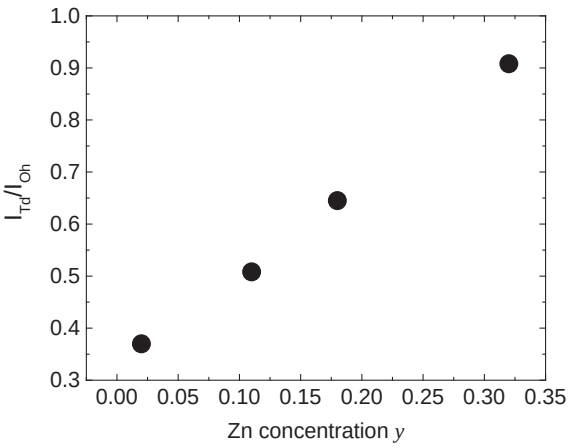

Figure 3-6 The composition dependence of PL intensity ratio (I_{Td}/I_{Oh}) at 80 K

3.5. Reference

[1] S. H. Tsai, S. Basu, C. Y. Huang, L. C. Hsu, Y. G. Lin, and R. H. Horng, *Sci. Rep.* **8** (2018) 1

[2] S. Itoh, H. Toki, Y. Sato, K. Morimoto, and T. Kishino, *J. Electrochem. Soc.*, **138** (1991) 1509

[3] T. Minami, T. Maeno, Y. Kuroi, and S. Takata, *Jpn, J. Appl. Phys.*, 34 (1995) L684

[4] H. W. Xue, Q. M. He, G. Z. Jian, S. B. Long, T. Pang, and M. Liu, *Nanoscale Res. Lett.*, **13** (2018) 1

[5] K. Ide, Y. Futakado, N. Watanabe, J. Kim, T. Katase, H. Hiramatsu, H. Hosono, and T. Kamiya, *Phys. Status Solidi Appl. Mater. Sci.*, **216** (2019) 1800198

[6] N. Watanabe, K. Ide, J. Kim, T. Katase, H. Hiramatsu, H. Hosono, and T. Kamiya, *Phys. Status Solidi Appl. Mater. Sci.*, **216** (2019) 1700833

[7] T. Miyata, T. Nakatani, and T. Minami, *J. Lumin.*, ***87–89*** (2000)1183

[8] E. Nogales, B. Méndez, J. Piqueras, and J. A. García, *Nanotechnology*, **20** (2009) 115201

[9] O. Muller, and R. Roy, “The Major Ternary Structural Families”, *Springer-Verlag* (1974) 38-54

[10] S. Yoshioka, H. Hayashi, A. Kuwabara, F. Oba, K. Matsunaga, and I. Tanaka, *J. Phys. Condens. Matter*, 19 (2007) 346211

[11] T. Chen, and K. Tang, *Appl. Phys. Lett.*, *90* (2007) 053104

[12] H. Hayashi, R. Huang, H. Ikeno, F. Oba, S. Yoshioka, I. Tanaka, and S. Sonoda, *Appl. Phys. Lett.*, 89 (2006) 181903

[13] T. Oshima, T. Nakazono, A. Mukai, A. Ohtomo, *J. Cryst. Growth*, **359** (2012) 60

[14] Y. Yuan, W. Du, and X. Qian, *J. Mater. Chem.*, **22** (2012) 653

[15] J. Liu, X. Duan, Y. Zhang, and H. Jiang, *J. Phys. Chem. Solids*, **81** (2015) 15

[16] Y. E. Lee, D. P. Norton, and J. D. Budai, *Appl. Phys. Lett.*, **74** (1999) 3155

[17] T. Oshima, M. Niwa, A. Mukai, T. Nagami, T. Suyama, and A. Ohtomo, *J. Cryst. Growth*, **386** (2014) 190

[18] L. E. Shea, R. K. Datta, and J. J. Brown, *J. Electrochem. Soc.*, **141** (1994) 1950

[19] T. K. Tran, W. Park, J. W. Tomm, B. K. Wagner, S. M. Jacobsen, C. J. Summers, P. N. Yocom, and S. K. McClelland, *J. Appl. Phys.*, **78** (1995) 5691

[20] J. S. Kim, J. S. Kim, T. W. Kim, S. M. Kim, and H. L. Park, *Appl. Phys. Lett.*, **86** (2005) 091912

[21] G. Bai, Y. Zhang, and J. Hao, *Sci. Reports*, **4** (2014) 5724

[22] R. D. Shannon, *Acta Crystallogr. Sect. A*, **A32**(5) (1976) 751

Chapter 4.

The observation of the luminescence from Manganese doped Zn_2SnO_4-Mg_2SnO_4 by tailoring band gap

4.1. Introduction

In this chapter, the experiment was conducted focusing on the change of the excitation wavelength with the film formation in chapter 2. The target material is $A_2SnO_4:Mn^{2+}$ (A = Mg, Zn) in which the presence or absence of light emission changes as the composition. Generally, $Zn_2SnO_4:Mn^{2+}$ did not show the luminescence at room temperature [1]. However, the green light emission was observed by Mg substitution increases in Zn_2SnO_4: Mn^{2+} [1, 2]. Recently, in rare earth metal doped garnet materials, it is revealed that the thermal quenching temperature is depending on a bandgap by changing host compositions [3, 4]. This reason is the change in the relative position of excited energy levels in the luminescent center with changing in the band gap depending on the compositions. Moreover, a lifetime in a persistent phosphor also can be changed by changing host compositions [5]. Therefore, it is important that tuning the bandgap of host compositions in phosphor materials. Several similar studies have been reported on spinel and perovskite materials as well as garnet materials [6-8]. Therefore, I focused on that changing the form to a thin film or nanoparticles increases the band gap of the material [9, 10]. Accordingly, it is an objective to observe the luminescence from the phosphor, which did not exhibit the luminescence at room temperature, by preparing the film.

4.2. Experimental Procedure

Composition-spread Zn_2SnO_4-$Mg_2SnO_4:Mn^{2+}$ (ZTO-MTO) film was prepared using combinatorial pulsed laser deposition. The Zn-excess $Zn_{2.985}SnO_4$ and Mg-excess $Mg_{2.985}SnO_4$ targets were synthesized by solid-state reaction method. The Mn/Sn ratio was fixed at 0.01. The ZnO, MgO, SnO_2, and MnO as raw materials were mixed with

ethanol in an agate mortar. The mixture was pelletized in 20 mm diameter and sintered at 1673 K for 6 h. Although the MTO target showed the green luminescence under UV irradiation, the emission was not observed in ZTO target.

The composition-spread film was deposited using combinatorial mask with a square hole (10×10 mm). Since the deposition rates of ZTO and MTO were 234 pulses/unit-cell and 155 pulses/unit-cell, respectively, the mask was moved along the longer direction of the substrate so that thicknesses at the edge of each thin film became a half of unit cell. The films were deposited at 773K under an oxygen pressure of 0.2 mTorr. The repetition and fluence of the laser were 10 Hz and 2.4 J/cm^2, respectively. The film thicknesses adjusted about 90 nm. The crystal structure of the films was characterized by high-resolution X-ray diffraction (HRXRD) using a Rigaku Smart-Lab diffractometer where X-ray was monochromatized using Ge(220) 2-bounce crystal and Cu$K\alpha_1$ radiation (λ=1.5406 Å). Zn concentration of the film was measured by an electron probe microanalyzer (EPMA). Positional dependence of Photoluminescence excitation (PLE) spectra was measured by spectrofluorometer (JASCO, FP-6500) with shadow mask (3× 3 mm) at room temperature. The detection wavelengths at every position were fixed at 499 nm.

4.3. Results and Discussions

4.3.1. Structure and composition analysis

The XRD diffraction patterns of compositional spread ZTO-MTO films were shown in Fig. 4-1. The films were grown epitaxially along *00l* direction of cubic spinel structure and secondary phase was not observed. The *004* diffraction peak of the substrate left unchanged while that of the film shifted with an increase in Mg substitution. Therefore, the lattice constant was calculated using Bragg's law and the result was shown in Fig. 4-2 with the composition of films characterized by EPMA. The EDX intensity of Zn ion almost linearly decrease along the longer direction of the substrate and reached to almost zero at around 7 mm from the edge of one side. Therefore, the film has a pure MTO area and the composition is gradually changed to ZTO. Based on the results of composition analysis, a lattice constant decreased with decreasing in the Zn concentration and the minimum value was observed at the same point where the Zn concentration reached almost zero. Therefore, this result indicated that the change in lattice constant was

reflected in the composition of the film. In the bulk ceramics, the lattice constant of ZTO (JCPDS No. 00-024-1470) and MTO (No. 00-024-0723) is 8.6570 Å and 8.6380 Å, respectively. In this study, the lattice constant of ZTO side was agreed with the value of bulk, but that of MTO side was smaller than that of MTO bulk ceramics. The reason for this change was considered to be that various defects (cations or oxygen) were introduced during the preparation of the films because the Zn and Mg have high vapor pressure [11].

4.3.2. Luminescent properties

Fig. 4-3(a) showed the images of the film irradiated by different wavelengths. The green luminescence was observed at around the center of the film in every excitation wavelength. This green luminescence was attributed to a transition from $^4T_1$ to $^6A_1$ of Mn^{2+} [1, 2]. It should be noted that the position where observed the most intense luminescence shifted to ZTO side. When the excitation wavelength was at 240 nm, the intense luminescence was observed at around the center of the film. By contrast, the area of the intense luminescence became narrow and shifted to ZTO side in the film irradiated by 280 nm. To reveal the cause of the change in the luminescent area depending on the excitation wavelength, the PLE spectra were obtained using the shadow mask. Fig. 4-3(b) showed that the positional dependence of PLE spectra monitored at 499 nm. “Area*x*" means that the position of the shadow mask, which corresponded to the measurement range from *x* to *x*+3 mm along longer side of substrate. The PLE spectra were obtained in areas form Area0 to Area5 and had a single peak. Usually, the PLE spectra in the Mn^{2+} doped spinel phosphor had two peaks which arose from the absorption of the host material and Mn^{2+}, respectively [12, 13]. In this study, the absorption of Mn^{2+} vanished and only the host absorption could be observed. The reason for this is thought to be the decrease in the amount of Mn ions because of the decreasing volume of phosphor the accompanying film formation. Therefore, the peaks that appeared at 219 – 245 nm were attributed to the host absorption.

4.3.3. Discussion

The intensity of PLE increased with an increase in MTO and decrease after reaching a maximum at Area3. Usually, Mn^{2+} doped ZTO does not exhibit the green luminescence

and the maximum intensity recorded from MTO [1, 2]. However, in this study, the ZTO-MTO film exhibited the different behavior with the bulk ceramics and the green luminescence was observed at ZTO side rather than MTO side. This result indicated that host absorption, that is, the band gap of the film was changed. As if to support this assumption, it was confirmed that the peak position of the PLE spectra was shifted to a lower wavelength side with an increase in MTO concentration (shown in Fig. 4-4). In the ZTO-MTO solid solution, since the excitation spectra corresponded to the band gap, it can be seen that the band gap increased in Fig. 4-4. Therefore, the band gap of ZTO-MTO increased by changing from the bulk to the film. The excitation level of Mn^{2+} is located under the conduction band in $ZnMgSnO_4$: Mn^{2+} bulk ceramics because the luminescence quenching was observed around its composition [1].

4.4. Summary

To summarize, I investigated the compositional spread ZTO-MTO film prepared by combinatorial PLD. The composition of the prepared film gradually changed from ZTO to MTO. Moreover, the lattice constant decreased with an increase in amount of Mg substitution. The films showed bright green luminescence. And the most intense luminescence was observed around the center of the sample. The emission intensity and the position of the most intense luminescence were changed by irradiated various excitation wavelengths. This cause was revealed by the positional dependence of PLE spectra. The PLE peak, which corresponded to host absorption, was larger than that of bulk material and increased with an increase in Mg substitution. Since the emission cannot usually be observed from Mn doped ZTO, I suggest that the luminescence from the prepared film was caused by an increase in the band gap because of the size effect.

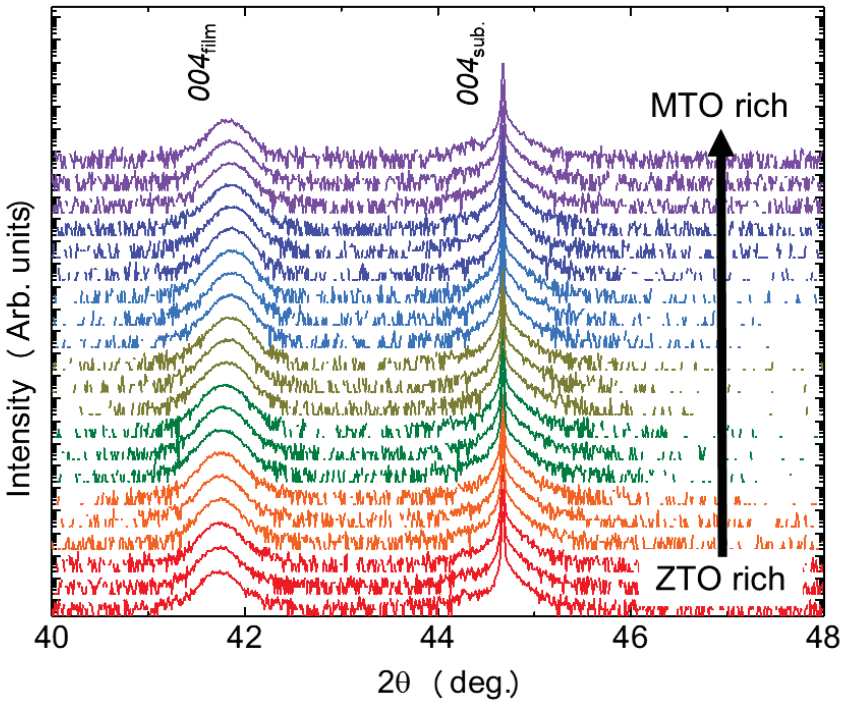

Figure 4-1. Positional dependence of XRD patterns

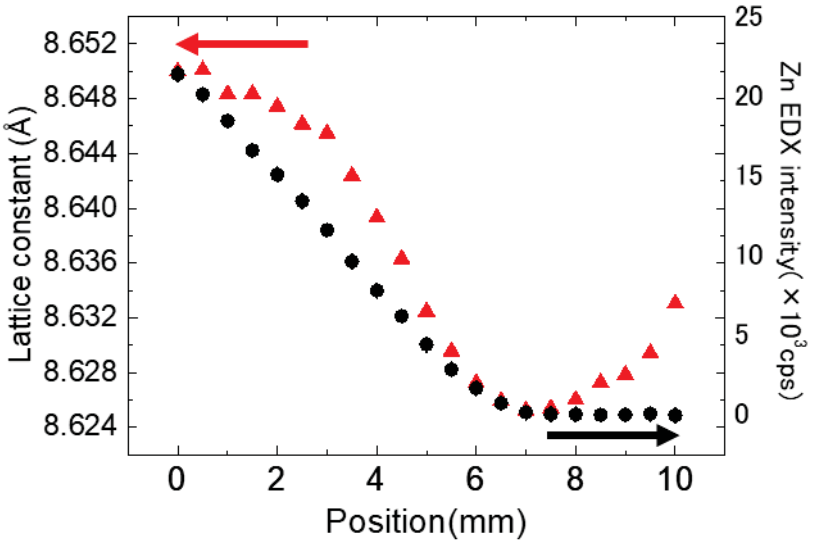

Figure 4-2. The lattice constant and Zn concentration of composition-spread film

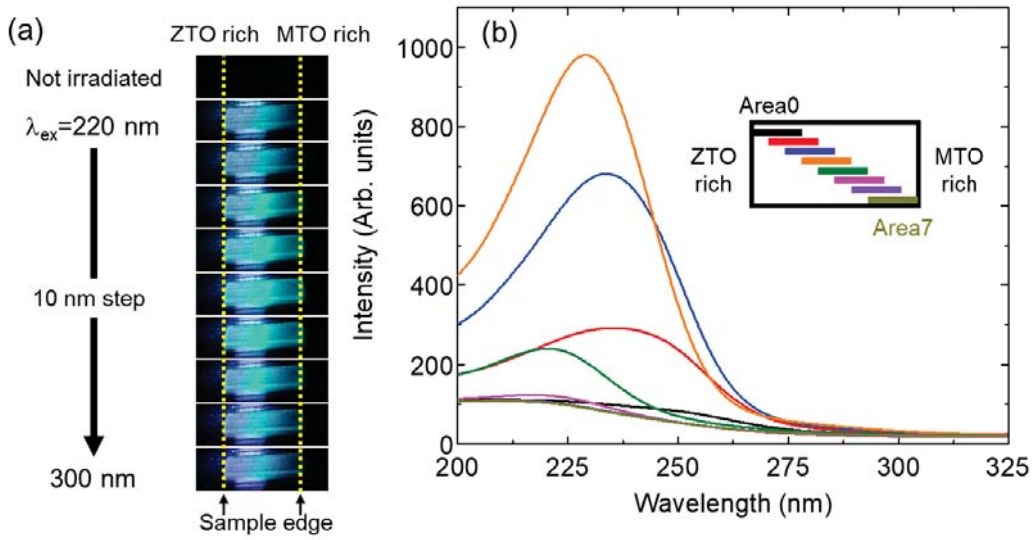

Figure 4-3. (a) Image of the film irradiated by different excitation wavelength, which changed every 10 nm from 220 nm to 300 nm. (b) The positional dependence of excitation spectra monitored at 499 nm.

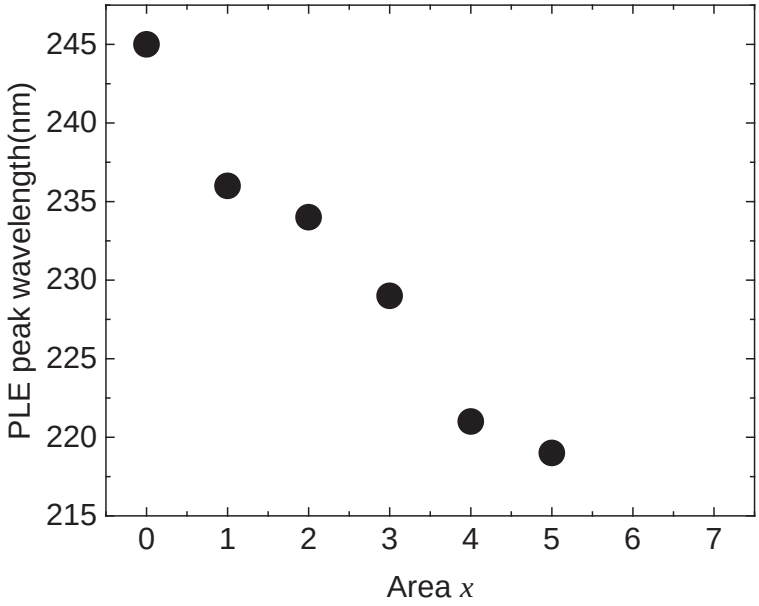

Figure 4-4. Positional dependence of PLE peak wavelength

4.5. Reference

[1] M. Kitaura, S. Tani, S. Mitsudo, and K. Fukui, *J. Vac. Sci. Technol. B.*, **28** (2010)

C2C20

[2] M. Kitaura, S. Tani, S. Mitsudo, and K. Fukui, *Radiat. Meas.*, **45** (2010) 503

[3] J. Ueda, S. Tanabe, and T. Nakanishi, *J. Appl. Phys.*, **110** (2011) 053102

[4] J. Ueda, A. Meijerink, P. Dorenbos, A.J.J. Bos, and S. Tanabe, *Phys. Rev. B.*, **95** (2017) 014303

[5] J. Ueda, K. Kuroishi, and S. Tanabe, *Appl. Phys. Lett.*, **104** (2014) 101904.

[6] Y. Zhuang, J. Ueda, and S. Tanabe, *J. Mater. Chem. C.*, **1** (2013) 7849

[7] P. Boutinaud, L. Sarakha, E. Cavalli, M. Bettinelli, P. Dorenbos, and R. Mahiou, *J. Phys. D. Appl. Phys.*, **42** (2009) 045106

[8] Y. Katayama, H. Kobayashi, J. Ueda, B. Viana, and S. Tanabe, *Opt. Mater. Express*, **6** (2016) 1500

[9] M.D. Benoy, E.M. Mohammed, M. Suresh Babu, P.J. Binu, and B. Pradeep, *Brazilian J. Phys.* **39** (2009) 629

[10] R. Rossetti, J.L. Ellison, J.M. Gibson, and L. E. Brus, *J. Chem. Phys.*, **80** (1984) 4464

[11] Y.E. Lee, D.P. Norton, and J.D. Budai, *Appl. Phys. Lett.*, **74** (1999) 3155

[12] B. Lei, B. Li, X. Wang, and W. Li, *J. Lumin.*, **118** (2006) 173

[13] C.F. Yu, and P. Lin, *J. Appl. Phys.*, **79** (1996) 7191

Chapter 5.

Conclusion

5.1. Conclusion

Spinel compounds have been used in various fields of application as a key material of ceramics due to their various attractive properties. There are a variety of interesting properties, such as electrical and magnetic properties, and I focused on the luminescent properties in this study. Although spinel oxide has been actively studied as a phosphor in bulk, whereas research on thin films, which are expected to be used for display devices, has not well progressed yet. Therefore, in this study, I investigated how the luminescent properties changed as a result of film formation, and searched for characteristics that are unique to thin films. In particular, the purpose of this study was to control the luminescence and the luminescence excitation wavelength by controlling the strain from the substrate and the composition of the thin film as it changes from the bulk to the thin film. I have shown that it is possible to adjust optical properties using compositional changes that were not previously possible in bulk material using thin film formation. By controlling the bandgap not only by composition but also by size effects, I found the composition with maximum luminescence intensity in a different composition from the bulk phosphor.

In chapter 2, the effect of residual strain on luminescent properties of $ZnGa_2O_4$:Mn thin films was investigated. High-quality epitaxial thin films were prepared on (100)$MgAl_2O_4$ single crystal substrates by PLD technique, and the residual strain from the substrate was controlled by changing the film thickness and oxygen pressure during fabrication. All films showed the green emission originated from Mn^{2+}. The films with various thickness prepared under 0.2 mTorr of were always constrained to $MgAl_2O_4$ substrate. On the other hand, the film prepared under 100 mTorr relaxed from the substrate with increasing thickness, and then it was revealed that the strain and relaxation state coexisted by reciprocal space mapping. When the strain of the film is constant, the emission peak is constant. On the other hand, the emission peak approached the unstrained bulk of approximately 505 nm with a decrease in residual strain in the film. Comparing the

emission characteristics of thin films prepared under two conditions, the emission peak is affected only by strain. This strain-induced peak shift was explained by the change in length between the Mn^{2+} ion and the surrounding oxygen ion. Therefore, it was suggested that the emission spectra can be tuned by a control of strain.

In chapter 3, the effect of Zn concentration in $ZnGa_2O_4$:Mn film on luminescent properties was investigated using advantage of the stabilization of γ-Ga_2O_3, which is a metastable phase that can be prepared by film formation. $ZnGa_2O_4$:Mn thin film with various Zn deficient was prepared by PLD method using ceramics target with several Zn concentration. All films had spinel structure and were grown epitaxially on (100)$MgAl_2O_4$ substrate. Zn/Ga ratio, *d*-spacing, and optical bandgap of the films increased with an increase in Zn concentration. All films without γ-Ga_2O_3 exhibited the green emission originated from Mn^{2+}. The emission spectra can be decomvoluted into two peaks corresponding to the difference between the site where the emission center is located (Oh site and Td site). From the temperature dependence of emission spectra, it was clarified that the emission from each site has a different thermal quenching temperature. In addition, since the Td peak emitted the light up to a higher temperature than the Oh peak, it was observed that the shape of the spectrum changed depending on temperature. The spectral shape was not only depended on temperature but Zn concentration. With an increase in Zn concentration, the luminescent intensity of the Td peak increased. This result was similar to the change in crystal-site engineering. Therefore, I suggested that it is possible that cation-deficiency induced crystal-site engineering.

In chapter 4, using the increase in the band gap due to film formation that was clarified in chapter 2, I attempted to search for the composition that can emit light from materials that emission cannot be observed in bulk. A_2SnO_4 (*A*=Mg, Zn) with spinel structure were selected as a target material. The compositional spread manganese doped A_2SnO_4 (ZTO or MTO) film prepared by combinatorial PLD. The composition of the prepared film gradually changed from ZTO to MTO, and the lattice constant decreased with an increase in Mg concentration. Bright green luminescence was observed, and the position of the most intense luminescence stood at the center of the sample. The most intense position shifted with a change in the irradiating excitation wavelengths. This cause was clarified by the positional dependence of excitation spectra. It was confirmed that the band gap of

prepared film corresponding to peak wavelength of excitation spectra was larger than that of bulk material and increased with an increase in Mg concentration. Usually, the emission cannot be observed from Mn doped ZTO. Therefore, I suggest that the luminescence from the prepared film was caused by an increase in the band gap because of the size effect due to film formation.

In summary, two types of oxide phosphor with spinel structure were successfully grown on the $MgAl_2O_4$ substrate in the film form using PLD technique. I found that $ZnGa_2O_4$: Mn as a well-known phosphor showed significant changes in light emission characteristics when manufacturing conditions change. In particular, it became clear that the change in luminescent characteristics due to film formation was able to adjust by the strain from the substrate. Moreover, Zn defective $ZnGa_2O_4$:Mn, which is difficult to prepare in bulk, indicated that cation deficiency can be induced crystal-site engineering. This suggests that the use of thin films could be one potential way to expand the scope of phosphor material exploration. Furthermore, the stannate spinel succeeded in discovering a new light-emitting composition using the knowledge gained through this research.

Therefore, it was revealed that the optical properties of transition metal doped phosphor can be controlled by using thin film and it was suggested that existing phosphors can be applied to FPDs such as EL and FED, and new fluorescent materials can be explored.

Supplementary

Supplementary 1

Thickness dependence of excitation peak (In chapter 2)

Fig.S1-1 and S1-2 show the excitation spectra of the films prepared under the different oxygen pressures. The peaks located at around 230 nm in Fig.S1-1 are attributed to the host absorption of $ZnGa_2O_4$. Another peak arose at around 280 nm in thicker films, originating from a charge transfer (CT) absorption of Mn-O or $d^5 \rightarrow d^4s$ transition band [1]. This peak could have been due to the increased amount of Mn^{2+} in the film with increased thickness. The host absorption peak shifts to a longer wavelength, and the intensity of Mn-O absorption peak increases with an increase of film thickness. Similar host-absorption behavior is confirmed in Fig.S1-2. However, the peak from CT absorption is weaker compared to the ZGO0.2 case, because the peak from host absorption was broadened, suggesting that peaks from CT absorption are buried in a peak from host absorption. Fig.S1-3 shows peak positions originated from host absorption as a function of film thickness. The peak positions of the excitation spectra shift to longer wavelengths with an increase of thickness regardless of the deposition pressure; however, the amount of change differs. The change of excitation peak position behaves differently than that of emission peak position. Figs. S1-4 show the emission peak positions as a function of residual strain in the films. The peaks of ZGO0.2 films are shifted to longer wavelengths even though the residual strain is constant. In contrast, the peaks of the ZGO100 films are shifted to longer wavelengths with a decrease of the residual strain. Hence, the shifts of excitation peak position are explained by the change of residual strain and the change of film thickness. One of the reasons for the different peak locations despite the almost identical strains may reflect the composition of the film. What I cannot understand using the above reasons is why emission peaks were shifted but excitation peaks were almost constant in ZGO0.2. This could be explained by the effect of film thickness, in other words, size effect [2]. Table S1-1 summarizes the effects of film formation on luminescent characteristics.

It is generally known that the grain size can be evaluated by powder XRD using Scherrer's formula [3]. When the grain size was defined as D, Scherrer's equation was,

$$D = \frac{K\lambda}{B\cos\theta} \quad \text{(S1-1)}$$

, Where λ is the X-ray wavelength, θ is the Bragg angle (half of the diffraction angle 2θ), and B is the Full-Width at Half-Maxim (FWHM) of diffraction peak. K is a Scherrer

constant, which value of 0.9 is usually used. Then, this equation was applied to Fig. 2-2 and an estimated grain size is shown in Fig. S1-5. In the ZGO100 films, the grain size was about 6 nm regardless of the film thickness. On the other hand, in the case of ZGO0.2, the grain size increased as the film thickness increased. The relationship between the peak position of the excitation spectrum and the grain size is shown in Fig. S1-6. From this figure, no relationship between the two could be identified. The size effect depends on the shape of material. When the material is nano-particle, the three-dimensional size effect is observed, which depends on the grain size. However, in this study, the material formed thin films. In view of this point, it is confirmed that the excitation spectra depend on not the grain size, but film thickness. In other words, the “size effect” in this study means “thickness effect” which is one-dimensional size effect.

Reference

[1] K. Uheda, T. Maruyama, H. Takizawa, and T. Endo, *J. Alloys Compd.*, **263** (1997) 60

[2] R. Rossetti, J. L. Ellison, J. M. Gibson, and L. E. Brus, *J. Chem. Phys.* **80** (1984) 4464

[3] P. Scherrer, *Nachr. Ges. Wiss. Göttingen*, **26** (1918) 98-100.

Table S1-1 Summary of effects on luminescence properties

	Excitation	Emission
ZGO0.2	Size and Strain effect	Strain effect
ZGO100	Size and Strain effect	Strain effect

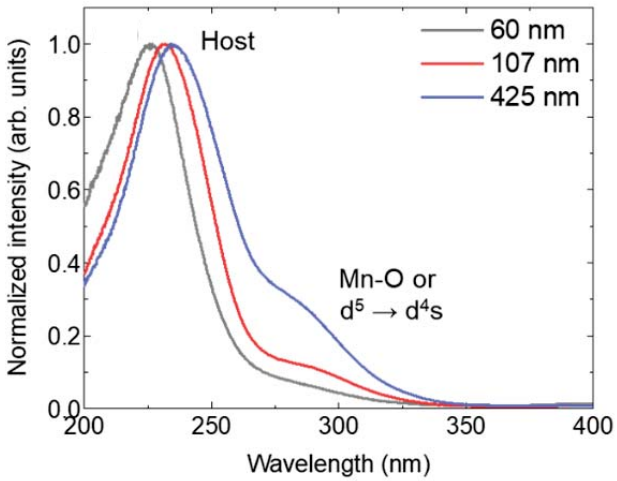

Fig.S1-1 Excitation peaks of ZGO0.2 with different thickness.

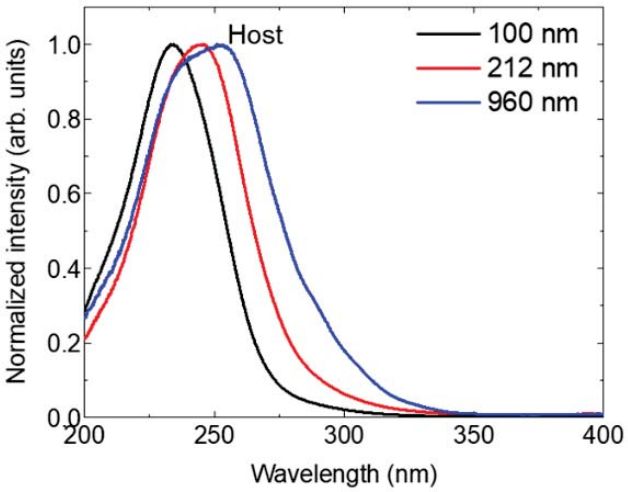

Fig.S1-2 Excitation peaks of ZGO100 with different thickness.

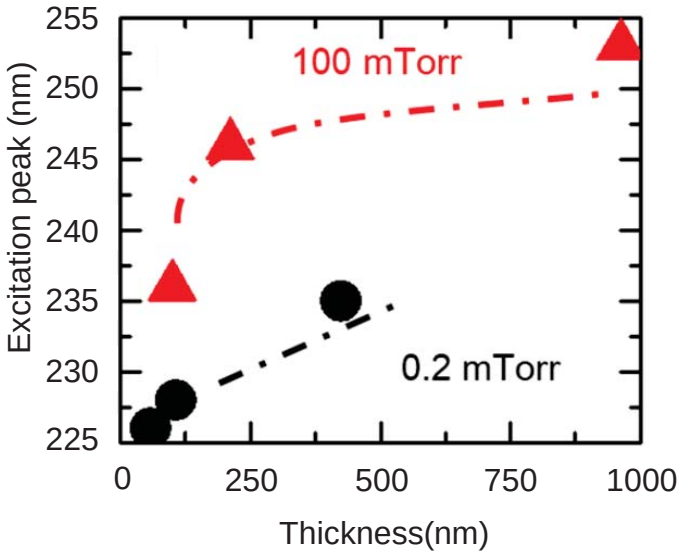

Fig.S1-3 Excitation peaks as a function of film thickness. The lines in the figure were drawn by eye guide.

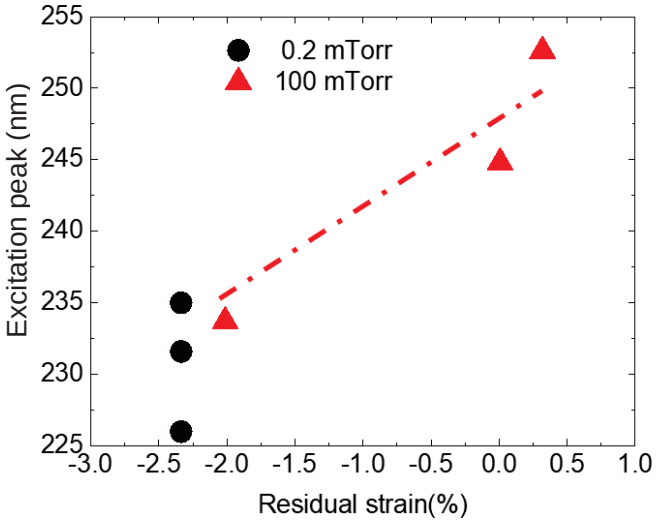

Fig.S1-4 Excitation peaks as a function of residual strain in the films. The lines are drawn by eye guide.

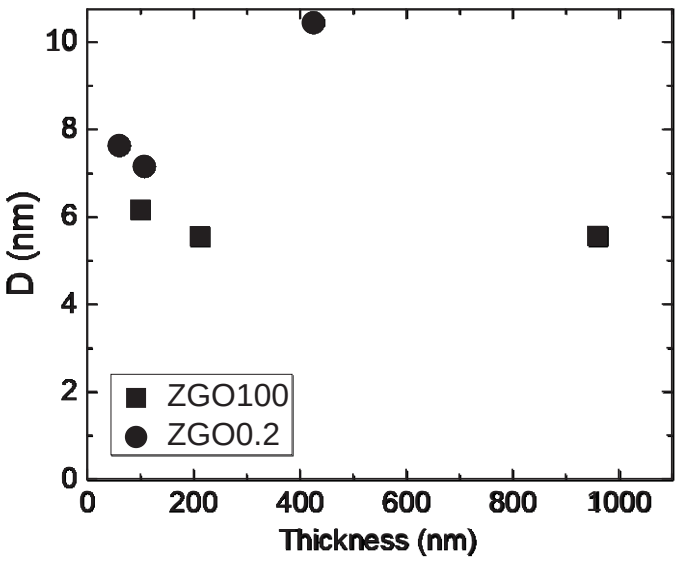

Fig. S1-5 Estimated grain size of ZGO100 and ZGO0.2 films

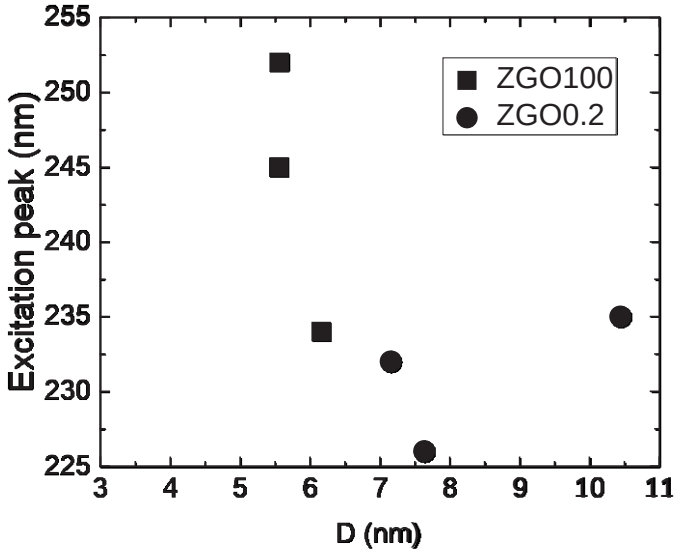

Fig. S1-6 Excitation peak position as a function of grain size.

Acknowledgment

The present study has been performed at the Itoh laboratory, Department of Materials Science and Engineering, Interdisciplinary Graduate School of Science and Engineering, Tokyo Institute of Technology for seven years from 2013.

First, I am deeply grateful Professor Mitsuru Itoh, my supervisor in my doctoral course, for their wonderful academic guidance, encouragement, and support that made this study meaningful and a successful. I would also like to sincere appreciation to Associate Professor Tomoyasu Taniyama (currently Professor in Nagoya University) who is my vice supervisor for useful advices and discussion. I would like to thank Assistant Professor Shintaro Yasui for his basic technical support and various advice during my research activities.

I would like to acknowledge Professor Fumiyasu Oba, Professor Hitoshi Kawaji, Associate Professor Hidenori Hiramatsu, Associate Professor Hiroyuki Wada, and Lecturer Akifumi Matsuda for useful advice to my doctoral thesis.

I am deeply grateful to Ms. Kozue Ando, the secretary who supported my research life.

I am delighted to have spent my research life with former laboratory members, Dr. Eiji Wada, Dr. Yasuhiro Shirahata, Dr. Ippei Suzuki, Dr. Yousuke Hamasaki, Dr. Katsuyoshi Komatsu, Dr. Tsukasa Katayama, Dr. Suseela Savitha Pillai, Dr. Zhang Minghui, Mr. Ryouta Shiina, Mr. Hidekazu Kojima, Mr. Yusuke Ishimoto, Mr. Masaki Tokunaga, Mr. Masayoshi Koga, Mr. Jumpei Okada, Mr. Han Yeifei, Mr. Takuya Miyauchi, Mr. Kazuki Ichikawa, Mr. Takuya Osakabe, Mr Ray Taniguchi, Mr. Toshiki Fujita, Mr. Taiki Noda, Mr. Ikuya Kokawa, and current members, Dr. RAO Badari Narayana Aroor, Mr. Takamasa Usami, Mr. Sou Yasuhara, Ms. Rika Itou, Mr. Koki Tachiyama, Ms. Miki Sato, Ms. Akiko Ito and Mr. Kent Teraguchi.

Finally, all I have to give my parents and brothers is my appreciation. It is thanks to you that I have enjoyed my research life so far.

List of publications and conference presentations

Publications related to the thesis

(1) **Takuro Dazai**, Shintaro Yasui, Tomoyasu Taniyama and Mitsuru Itoh, "Cation-deficiency induced crystal-site engineering for $ZnGa_2O_4:Mn^{2+}$ thin film" *Inorg. Chem.*, ***59*** (2020) 8744-8748.

(2) **Takuro Dazai**, Shintaro Yasui, Tomoyasu Taniyama and Mitsuru Itoh, "Epitaxial strain engineering of luminescent properties in $ZnGa_2O_4$:Mn thin film", *Appl. Phys. Express* **13** 082004.

(3) **Takuro Dazai**, Shintaro Yasui, Tomoyasu Taniyama and Mitsuru Itoh, "Bandgap tuning and optimization of green emitting Zn_2SnO_4-Mg_2SnO_4: Mn^{2+} using combinatorial pulsed laser deposition technique" Ceram. Int., (2020) *In press.*

Other publications

(1) Koki Tachiyama, Shintaro Yasui, Badari Narayana Aroor Rao, **Takuro Dazai**, Takamasa Usami, Tomoyasu Taniyama, Tsukasa Katayama, Yosuke Hamasaki, Jianding Yu, Huan He, Hui Wang, and Mitsuru Itoh* "Magnetic properties of Single Crystal $GaFeO_3$" MRS Adv. **4**(2019) 61.

International conference presentations

(1) **Takuro Dazai**, Shintaro Yasui, Tomoyasu Taniyama, and Mitsuru Itoh, The 13th Pacific Rim Conference of Ceramic Societies (PACRIM 13) (Okinawa, Japan), Temperature Dependence of the Emission Spectra Shape in Zn Deficient $ZnGa_2O_4$:Mn Film (Oral), Oct. 2019

(2) **Takuro Dazai**, Shintaro Yasui, Tsukasa Katayama, Tomoyasu Taniyama, and Mitsuru Itoh, The 11th International Conference on the Science and Technology for Advanced Ceramics (STAC-11) (Tsukuba, Japan), The Luminescent Property of $Pr_{0.002}(Sr_{0.4}Ca_{0.6})_{0.997}TiO_3$ Free Standing Film (Poster), July 2019

(3) Shintaro Yasui, Koki Tachiyama, Tsukasa Katayama, **Takuro Dazai**, Yosuke Hamasaki, Huan He, Hui Wang, Jianding Yu, and Mitsuru Itoh, 2018 MRS Fall

Meeting (Boston, USA), Preparation of *k*-Al_2O_3-Type Ferroelectric Single Crystal and Single Domain Epitaxial Thin Film and Their Properties (Oral), Nov. 2018

(4) K. Tachiyama, T. Katayama, T. Osakabe, **T. Dazai**, J. Yu, H. He, H. Wang, Y. Hamasaki, S. Yasui, T. Taniyama, and M. Itoh, 2018 ISAF-FMA-AMF- AMEC- PFM Joint Conference (IFAAP 2018) (Hiroshima, Japan) , Preparation of $GaFeO_3$ Single Crystal and Epitaxial Thin Films on Single Crystal (Oral), May 2018

(5) **Takuro Dazai**, Shintaro Yasui, Tomoyasu Taniyama, and Mitsuru Itoh, PRiME 2016 (Honolulu, Hawaii), Co-Doped Effect of Afterglow Properties in $R_3GaO_6:Eu^{3+}$ (*R* = Y, Gd) (Oral), Oct. 2016

(6) **T. Dazai**, Y. Hamasaki, S. Yasui, T. Taniyama, and M. Itoh, The 9th International Conference on the Science and Technology for Advanced Ceramics (STAC-9) (Tsukuba, Japan), Changing of the Excitation Wavelength of Scheelite Type Oxide Thin Films (Poster), Oct. 2015

(7) **T. Dazai**, Y. Hamasaki, S. Yasui, T. Taniyama and M. Itoh, 13th International Ceramics Congress (CIMTEC 2014) (Montecatini Terme, Italy), Growth Control of Epitaxial $CaMoO_4$ Thin Films by Pulsed Laser Deposition (Poster), June 2014.

Domestic conference presentation

(1) **T. Dazai**, Y. Hamasaki, S. Yasui, T. Taniyama and M. Itoh, ” Preparation of CaMoO4 epitaxial films by PLD method and their luminescence properties” (Oral), The Ceramic Society of Japan, The 52nd symposium on Basic Science Division, Nagoya, January 2014.

(2) **T. Dazai**, Y. Hamasaki, S. Yasui, T. Taniyamam, H. Takashima and M. Itoh, “Characterization of Scheelite-type oxide phosphor thin films” (Poster), The Ceramic Society of Japan, The 27th Fall Meeting, Kagoshima, September 2014.

(3) **T. Dazai**, Y. Hamasaki, S. Yasui, T. Taniyama and M. Itoh,” Afterglow properties of $Ln_3GaO_6:Eu^{3+}$ red phosphor” (Oral), The Ceramic Society of Japan, Annual Meeting, Tokyo, March 2016.

(4) **T. Dazai**, S. Yasui, T. Taniyama and M. Itoh, "Effect of co-doping elements in $Y_3CaO_6:Eu^{3+}$ red afterglow phosphor" (Poster), The Japan Society of Applied Physics, The 77th Fall Meeting, Nigata, September 2016.

(5) **T. Dazai**, S. Yasui, T. Taniyama and M. Itoh, "Effect of doping elements on the afterglow properties of red phosphor $Y_3GaO_6:Eu^{3+}$"(Poster), The Ceramics Society of Japan, The 6th Young Researchers Meeting of The Kanto Branch, Yokohama, November 2016.

(6) **T. Dazai**, S. Yasui, T. Taniyama and M. Itoh, "Effects of Zn concentration on the luminescent properties of spinel-type $ZnGa_2O_4$:Mn phosphor films"(Oral), The Ceramic Society of Japan, Annual Meeting, Miyagi, March 2018.

(7) **T. Dazai**, S. Yasui, T. Katayama, T. Taniyama and M. Itoh, "Preparation of free standing PSCTO single crystal thin films of water-soluble $Sr_3Al_2O_6$ and their luminescent properties"(Oral), The Japan Society of Applied Physics, The 66th Spring Meeting, Tokyo, March 2019.